

## **Tectonic Appraisal of the Mid-Thane Creek of Mumbai, India:**

### **An Integrated Geophysical Approach**

**J. Jacob<sup>1,2\*</sup>, P.V. Kumar<sup>1</sup>, K.M. Dubey<sup>1,3</sup>, A. Mishra<sup>1,4</sup>, P. Kumar<sup>1,4</sup>, S. Kumar<sup>1,5</sup>, V.P. Mahale<sup>2</sup>, A.K. Chaubey<sup>1</sup>**

<sup>1</sup>CSIR- National Institute of Oceanography, Regional Center, Lokhandwala Road, Andheri (West), Mumbai-400053, Maharashtra, India.

<sup>2</sup>CSIR-National Institute of Oceanography, Dona Paula, Goa-403004, India

<sup>3</sup>Department of Marine Sciences, Goa University, Taleigao Plateau, Goa-403206, India

<sup>4</sup>Academy of Scientific and Innovative Research, CSIR-National Institute of Oceanography, Goa, India

<sup>5</sup>Department of Geophysics, Banaras Hindu University, Varanasi- 221005.

\*Corresponding author

Email: jacob@nio.org; jensensaviojacob@gmail.com

#### **Abstract**

Integrated geophysical surveys, comprising marine magnetic, high resolution shallow seismic and single-beam bathymetry were conducted to assess subsurface tectonics of the Mid Thane Creek (MTC) of Mumbai. The bathymetry in the intertidal zone of MTC varies drastically due to periodic dredging, with maximum depth up to 6.4 m and a minimum of -1.6 m. High resolution shallow seismic sections up to the depth of ~35 m from the sea-floor are generated to analyze the neotectonic activity of the creek. Imprints of deep-seated lineaments are recognized from magnetic anomaly map of the MTC. To delimit lateral extent of the lineaments/faults, results of several derivative methods including tilt derivative and standard Euler deconvolution are merged with the selected crest value of the horizontal derivative. To estimate depth to the source, Euler deconvolution, tilt derivative, analytic signal, and source parameter imaging method have been used. However, the depth estimation for the lineaments/fault is highly discrepant for this region, because of the complex tectonics associated with the periodic emplacements of Deccan flood basalt. To confine the top and bottom boundary of this highly magnetized basaltic layer, we have carried out spectral analysis considering 18 windows of 2000x2000 m with an overlap of 500 m. The average depth to the top and bottom of the source body estimated using spectral analysis is consistent with the depth estimated from the derivative filters. This confirms that the lineaments identified by the derivative filters may embed in the basaltic layer of MTC. The most prominent lineament interpreted from the seismic and magnetic data, in the central region of MTC is inferred as the marine analog of Alibagh-Uran fault passing through the mainland of Alibagh and Uran close to Mumbai city.

**Key Words:** Thane creek; Marine magnetic; High resolution shallow seismic; Single beam bathymetry; Source depth; Flood basalt thickness, Spectral analysis.

#### **Key Points:**

- Acquired, processed and interpreted high resolution shallow seismic, marine magnetic, single beam bathymetry data in the Mid-Thane creek of Mumbai, India.
- Neo-tectonic and deep-seated tectonic elements are identified using the seismic and magnetic data.
- Identification of the faults/lineaments and source depth estimation are performed using Total Horizontal, Analytic signal, Tilt Derivative, Euler Deconvolution and Source parameter imaging derivative methods.
- Thickness of the flood basalt where the faults/lineaments are embedded is estimated using spectral analysis.
- Interpreting the marine extension of Alibagh-Uran fault zone in the Mid-Thane creek of Mumbai, India

## 1 Introduction

The commercial prominence of Thane creek has been emphasized over centuries as the creek serves as navigational channel for Mumbai harbor for trade and transportation. Over decades with the rapid urbanization of Mumbai city, the harbor has expanded to present Mumbai Port along with the establishment of India's largest container port, Jawaharlal Nehru Port, on either flank of the Thane creek. Considering the proximal and convenient location, Thane creek serves as a water link between main land Mumbai and Navi Mumbai, expanding the industrialization on the peripheries of the creek. Due to continuous anthropogenic interference, Thane creek is continuously monitored for several ecological aspects (e.g. Ram et al., 2009; Quadros et al., 2009; Fernandes et al., 2012). However, geophysical investigations and tectonic studies of the creek are very sporadic compared to the extensive studies and documentations on the counterpart continent (Rajaram et al., 2016). Many of the prominent faults and lineaments identified on land, whose offshore extent is not demarcated, may continue towards the continental shelf, traversing the Thane creek. Understanding these probable weak zones is important for the efficient planning, execution and durability of engineering structures, and tectonic evaluation in and around the Thane creek. In this study we investigate some of the tectonic elements in the Mid-Thane Creek (MTC), including both the neo-tectonics and deep-seated weak zones, if any, integrating bathymetry, high resolution shallow seismic and magnetic studies.

## 2 Tectonic Attributes of MTC

Ghodke (1978) interpreted the prominent fault zone of Alibagh-Uran trending N35°E at Alibagh and striking N-S at Uran. Along the fault at Uran the lava flows have higher dip (25° W) and regain the low dip angle of 10° on the western as well as eastern flank of the ~25m wide fault zone, indicates the block rotation of the basalt dykes adjacent to the fault zone. Towards the northern extent near Alibagh, the fault zone widens ~200 m with a dip angle of 40° E. Ghodke 1978 suggested that the Nhava-Sheva Fault and the Belpada Fault lying east of the Alibagh-Uran Fault have the same N-S trend and eastward down throw of ~30 m to ~60 m, which has been later confirmed by Dessai and Bertrand, (1995). Though a general en-echelon pattern of eastward dipping parallel/sub-parallel fault system is generally depicted along the passive rift margin of western Maharashtra, Srinivasan 2002 has identified the Mahim fault north of Mumbai characterized by westward step faulting whose southern end passes through Uran and Nhava-Sheva. However, previous studies of Dessai et al. (1990) interpreted the NW-SE trending Uran-Dabhol lineament as dike swarm. Samant et al. (2017) identified two prominent normal faults at ~70 m apart, the Western fault and Eastern fault on the Elephanta Island. The Western fault trends N25°E with an average dip angle of 65°, while the Eastern

fault has a strike direction of N36<sup>0</sup>E dipping at 73<sup>0</sup>. Apparently, the faults have undergone an oblique slip movement with localized block rotations indicating a listric fault pattern. The linear trend and the consistent eastward down throws of the Alibagh-Uran Fault and Elephanta Faults, suggested that the faults are in close proximity, they could be of a single fault system. The detailed tectonic framework of MTC is shown in Figure 1.

The West Coast Fault (WCF) trending NNW, fringing the western flank of Maharashtra, follows the NNW-SSE trend of Precambrian basement of Dharwar (Biswas, 1987; Gombos et al., 1995). Though the exact location of this prominent fault system is on debate, the WCF is considered as the consequences of the early extensional regime of Gondwana breakup preceding the separation of India from Seychelles (Dessai and Bertrand, 1995; Mukherjee et al., 2017). The WCF is supposed to be formed in two stages (Chandrasekharam, 1985), the initial northern fracturing during late Jurassic-Early Cretaceous (Owen, 1976; Biswas, 1982) could be associated with the early rifting episode between India and Madagascar at ~84 Ma (Bhattacharya and Yatheesh, 2015). The later extension of the fracture towards the south during the Tertiary (Owen, 1976) is associated with the rifting stage between India and Seychelles.

A prominent dip of 17° W is observed by Wynne 1886 on the basaltic emplacements of the continental flank of Maharashtra. However, Auden 1949 named this seaward dipping phenomenon as “Panvel Flexure”. Several studies have been carried out to examine the structure and origin of Panvel Flexure. Many studies proposed, Panvel flexure as 1) “monoclinical flexure” associated with the initial rifting and the uplift of Western Ghats (e.g. Wynne, 1886; Devey and Lightfoot, 1986; Watts and Cox, 1989), 2) block rotation of fault blocks in extensional regime (e.g., Dessai and Bertrand, 1995), and 3) listric fault with reverse drag structure (Sheth, 1998). The tectonic association of WCF with rifting episodes of the western margin of India is explicated from the ~30 km wide Panvel flexure which dissects the entire Deccan trap for ~150 km, following NNW-SSE trend of the western Indian passive margin (Dessai and Bertrand, 1995; Sheth, 1998). The age of Panvel flexure is not precisely demarcated, but several studies suggested more or less a contemporaneous age of Deccan volcanism. The influence of Panvel flexure extends to the Deccan basalts with a dip angle of 2°-5°W, covering the Navi Mumbai and Nhava–Sheva–Uran areas, until the lava flows shows a horizontal trend in the east (Samant et al., 2017).

Offshore extension of the flood basalt up to the Laxmi Ridge is reported by Kumar and Chaubey (2019). The Elephanta Island manifests the offshore emplacement of the Deccan flood basalt situated ~3 km from the Mumbai harbor. The island is elevated ~168 m on the eastern side and ~131 m on the western side above mean sea level, showing ~12<sup>0</sup> WNW dip (Sheth and Samant, 2016). The

coastal tholeiitic dyke intrusions show a varying trend from N-S, NNW-SSE and majority trending in NNE-SSW direction, which implies ESE-WNW extensional regime for the rifting episodes (Dessai and Bertrand, 1995; Sheth and Pande, 2014; Samant et al., 2017).

### **3 Regional Geology**

Thane creek and surrounding region are affected by the Deccan flood basalt emplacement that was formed by volcanic effusions within a narrow time span of 65-69 Ma (Courtillot et al., 1986; Duncan and Pyle, 1988). The central part of the survey area is surrounded by Trombay, Butcher, Elephanta, Nhava and Sheva islands. Lithostratigraphically, Trombay island falls in Mumbai island formation of Salsette subgroup (Sethna, 1999) whereas Nhava and Sheva Island falls under the Bushe Formation and the land part east of the Nhava Island falls in Khandala Formation of Lonavala Subgroup. The land part southwest of Uran (near Mandve) falls under Poladpur Formation of Wai Subgroup, which is younger than Bushe and Khandala formations (Choudhary and Jadhav, 2014). These islands are mainly made up of pahoehoe type lava flow and at some place rubbly lava flow. Pahoehoe lava flow suggests that these islands have been formed in subaerial condition. The survey area and peripheral region is a highly tectonized and characterized by varied magmatism (Sheth and Chandrasekharam, 1997a, 1997b). All the islands in the vicinity of the survey area are made up of vesicular lava flow, which mainly consist of basalt along with porphyrite, tholeiites, trachytes and rhyolites (Lightfoot et al., 1987). Spilites, pillow basalts and basalts inter-layered with sediments at Bombay indicate that the area was undergoing active subsidence throughout the volcanic episode (Sethana, 1999). Different geologic formations of MTC are represented in Figure 1.

### **4 Geophysical Data**

Thane creek, fringing the eastern flank of Mumbai city is connected to Ulhas River at north. Panvel creek merges at the middle stream of the Thane creek where Butcher and Elephanta islands are the prominent landmarks. The final stage of the creek at southern extremity opens into the Arabian Sea. The survey area is located in middle stream of the Thane creek (Fig. 2). We refer the study area as Mid-Thane Creek (MTC), which is limited by the Trombay hills in the northwest, and islands of Butcher, Elephanta, Nhava-Sheva in the south. The eastern extreme of the study area extend up to the mouth of the Panvel creek, while the Sewri fort and Mumbai port limits the western end. Considering bathymetry records from the National Hydrographic Office (NHO), initial planning and execution of data acquisition is accomplished. Assessing the navigational difficulties due to fluctuating water depths associated with the tidal variations in the creek, the survey area is divided into sectors; Sector 1 (western part of the of the survey area), Sector 2 (Central region of the survey

area), and Sector 3 (eastern part of the survey area). Maximum water depth recorded is 6.4 m near the Trombay channel region and the minimum depth of -1.6 m is recorded in the western part of the creek, in intertidal zone. Hence Sectors 1 and 3 were surveyed exclusively during high tides, as the seabed gets exposed during low tides. Bathymetry survey was carried out in MTC synchronized with the seismic and magnetic surveys. Atlas Deso-30 dual channel (33/210 kHz frequency) and Bathy-500 MF (210 kHz frequency) echo-sounders were used for bathymetry data acquisition and HYPACK® software is used for processing the data. After applying tidal correction, data were reduced to chart datum. The processed depth data is gridded at an interval of 10 m to produce gridded bathymetry map of the MTC.

High resolution shallow seismic survey was carried along 7 track lines with 20 m track spacing, traversing MTC using Sparker seismic data acquisition system. The entire unit of sparker system includes CSP D700 energy source, multi-tips squid spark array, data acquisition unit Octopus 760 and a 20 element hydrophone arrays with 0.25 m hydrophone spacing. The energy source has been calibrated to 100 joules per shot with sampling frequency of 24 kHz, to acquire the data in the frequency band of 250–2500 Hz. Position of the sparker system is synchronized with the survey boat using Differential Global Positioning System (DGPS) manufactured by Trimble (Model SPS 461) along with differential beacons (operating in 283.5–325 kHz band). Seismic data processing is performed using the software package SeisSpace®ProMAX® of Landmark Solutions. The data, resampled at 0.1 millisecond interval, has undergone trace editing to eliminate the erroneous seismic traces. Further, top muting is performed to eliminate direct arrivals and noise present in the water column. The quality of seismic reflectors is improved by applying band pass filtering, deconvolution and gain correction. The depth conversions are achieved by considering the P-wave velocities of 1500 m/s for water column and 1583 m/s for shallow sedimentary layers (Krishna et al. 1989).

Magnetic data were acquired along 7 track lines at 500 m track spacing on the northern region of the MTC. The survey was extended towards south of the Elephanta island, where additional ten survey lines were acquired keeping the same track line specifications. Total intensity of the earth's magnetic field in the Thane creek is recorded at an interval of 100 ms using Geometrics G-882 Cesium Vapor marine magnetometer. The magnetometer is interfaced with MagLog Lite software to log and print the magnetic data synchronized with Differential Global Positioning System (DGPS). Distance between the tow-fish and the DGPS antenna is measured for each survey line for appropriate layback corrections. The initial data is corrected by removing the high amplitude spikes associated with transient noise during the data acquisition. To generate the Total Magnetic Intensity (TMI) map (Fig. 3a), IGRF value (International Geomagnetic Reference Field) is subtracted from the total intensity of

the earth's magnetic field and gridded at an interval of 125 m. However, for detail analysis of magnetic data, several data enhancement techniques are performed on the magnetic anomaly data. The entire filtering procedures on TMI are carried out in frequency domain by Fast Fourier Transform (FFT). The magnetic anomaly measured at a specific location is highly dependent on inclination and declination of the Earth's magnetic field (Baranov, 1957), which may affect the accurate location and shape of the anomaly signal. Reduction to Pole (RTP) technique is applied to TMI with inclination of 27.6° and declination of -0.4° (Fig. 3b). Additional filtering and analysis techniques for identifying the contacts and depths of the lineaments/faults are applied to the RTP magnetic anomalies. To locate the lineaments with more precision and to estimate the source depth, comparison of the results from multiple techniques have been implemented.

## 5 Methodology: Lineaments Delineation and Source Depth Estimation

### 5.1 Total Horizontal Derivative Method (THD)

To locate the contact location of the lineaments/faults, we have considered total horizontal derivative method. The amplitude of the total horizontal gradient  $(\partial M / \partial h)$  of magnetic field (M) is high at the magnetic anomaly source contact. The horizontal gradient function assumes that the magnetic anomaly for an isolated vertical contact is measured in a vertical regional magnetic field with vertical magnetization. The total horizontal gradient of a magnetic field is defined as the sum of the derivatives in x- and y- directions (Phillips, 1998); hence the response of  $\partial M / \partial h$  to the noise is reduced.

$$\partial M / \partial h = \sqrt{(\partial M / \partial x)^2 + (\partial M / \partial y)^2}$$

### 5.2 Analytic Signal (AS)

The advantage of AS is that it is independent of magnetization direction (inclination) and provides both the vertical and horizontal derivatives in all possible direction of source magnetization (Nabighian, 1972). Hence, the amplitude of AS is high where the magnetic susceptibility contrast is maximum, which is represented as a bell-shaped symmetric function located directly above the source body. Roest et al. (1992) further considered the analytic signal in 3D scenario, where the amplitude of analytic signal (A) of a magnetic field (M) at a specific location (x, y, z) is described as the square root of the sum of the squares of the derivatives in x, y and z directions.

$$|A(x,y)| = \sqrt{(\partial M / \partial x)^2 + (\partial M / \partial y)^2 + (\partial M / \partial z)^2}$$

We have used AS to estimate the source depth in the MTC. The depth estimation of the magnetic anomaly source is performed by assigning different structural indices (N) for the ratio of analytic signal to vertical derivative of analytic signal ( $\partial AS$ ) using following formula:

$$\partial AS = \sqrt{(\partial M1/\partial x)^2 + (\partial M1/\partial y)^2 + (\partial M1/\partial z)^2}$$

Where  $\partial M1$  is the first vertical derivative of the total magnetic field. Structural index is the measure of rate of change of the magnetic field with distance. The structural index corresponds to geometry associated with respective tectonic element. For total magnetic anomaly, N=0 for contacts or steps, N=1 for dykes, N=2 for vertical pipe, N=3 for spherical anomaly source. Depth (D) of the source body is derived as (Reid et al., 1990):

$$D = \left( \frac{|A(x, y)|}{\partial AS} \right)^{1/N}$$

### 5.3 Tilt Derivative (TD)

The Tilt angle method (Miller and Singh, 1994; Verduzo et al., 2004) is used to locate the source of the magnetic anomaly by dividing the vertical derivative ( $\partial M/\partial z$ ) with total horizontal derivative ( $\partial M/\partial h$ ) of the magnetic anomaly (M), thereby eliminating the effect of induced magnetization of the source body.

$$\theta = \tan^{-1} \frac{\partial M/\partial z}{\partial M/\partial h}$$

Where  $\theta$  is the tilt angle, and

$$\partial M/\partial h = \sqrt{(\partial M/\partial x)^2 + (\partial M/\partial y)^2}$$

Tilt function has many intrinsic advantages as the value of tilt amplitude always falls between  $-90^\circ$  and  $+90^\circ$ . Salem et al. (2007) proposed the method to estimate the depth of the magnetic source using tilt angle ( $\theta$ ).

$$\theta = \tan^{-1} \frac{h}{z}$$

Where  $h$  is the horizontal distance measured from the horizontal location of the contact and  $z$  is the depth to the top of the contact. When  $h=0$  the tilt angle represents the zero-contour value, corresponds to or close to the edge of the magnetic source body, which is used to detect the source edge directly. The positive tilt angle contour values lie over the source body while the negative contours are outside the influence of the source body. Additionally, the depth value can be estimated by measuring the horizontal distance between  $0^\circ$  and  $45^\circ$  contour which is analogous to half the distance between  $\pm 45^\circ$  contours.

#### 5.4 Standard Euler Deconvolution (SED)

Standard Euler Deconvolution (SED) method, based on the Euler's homogeneity equation, used to locate and estimate the depth of the magnetic source (eg: Thompson, 1982; Reid et al., 1990; Stavrev, 1997; Barbosa et al., 1999). This method utilizes the concept of the degree of homogeneity as various structural indices ( $N$ ) are associated with different magnetic sources. For example, for total field magnetic anomalies,  $N=0$  for contact/step,  $N=1$  for dykes/sills,  $N=2$  for cylinder/pipe,  $N=3$  for sphere. The concept of Euler's homogeneity equation is derived by Thompson (1982).

$$(x - x_0) \frac{\partial M}{\partial x} + (y - y_0) \frac{\partial M}{\partial y} + (z - z_0) \frac{\partial M}{\partial z} = N (B - M)$$

Where  $M$  is the observed magnetic field at  $(x, y, z)$  and  $x_0, y_0, z_0$  are the position of the source body.

$\frac{\partial M}{\partial x}, \frac{\partial M}{\partial y}, \frac{\partial M}{\partial z}$  are the first order derivatives of the magnetic field in  $x, y$  and  $z$  directions, respectively.  $N$  is the structural index or the negative of the degree of homogeneity.  $B$  is the base value of TMI (regional magnetic value at  $(x, y, z)$ ).

The advantage of SED is that it does not require any prior knowledge of the source magnetization and is least affected by the remnant magnetization. But, the accuracy of the depth estimation is highly depending up on the appropriate selection of the structural index.

#### 5.5 Source Parameter Imaging (SPI)

Source parameter imaging method is based on the principle of complex analytic signal, known as local wavenumber ( $K$ ), for computing the depth of the source body. In classical SPI method (Thurston and Smith, 1997), for a dipping contact, the wavenumber is maximum ( $K_{max}$ ) over the source contact. The wavenumber  $K$  for a given magnetic field ( $M$ ) is defined as:



$$K = \frac{\frac{\partial^2 M}{\partial x \partial z} \frac{\partial M}{\partial x} - \frac{\partial^2 M}{\partial x^2} \frac{\partial M}{\partial z}}{\left(\frac{\partial M}{\partial x}\right)^2 + \left(\frac{\partial M}{\partial z}\right)^2}$$

$K_{max}$  is defined as the peak value of the wave number  $K$  over the magnetic source, represented as the maximum slope of the tilt angles. The tilt derivatives operate as edge detecting filter in SPI method as per following:

$$K_{max} = \sqrt{\left(\frac{\partial Tilt}{\partial x}\right)^2 + \left(\frac{\partial Tilt}{\partial y}\right)^2}$$

The depth of the source body is defined as the reciprocal of  $K_{max}$ .

$$Depth = \frac{1}{K_{max}}$$

However, the depth estimations using SPI is independent of magnetic inclination, declination, dip, strike and any remnant magnetization.

## 6 Results and Analysis

### 6.1 Bathymetry of MTC

We have integrated our field acquired single beam bathymetry data with the bathymetry data provided by National Hydrographic Office (NHO) of India, to increase the data resolution and coverage of MTC. The seabed of the creek is often disturbed by the periodic dredging for deepening of the navigational channels of Mumbai Port and Jawaharlal Nehru Port. The creek is manifested by the Sewari mud flat in the west and Nhava-Sheva mud flat in the east. The bathymetric profile between these two mud-flat regions extending from west to east is anomalous with undulating depth (Fig. 4a). The region east of the Pir Pau jetty shows two depressions on the seabed. These depressions correspond to dredged region near the Pir Pau turning circle and Trombay shipping channel, further east of the Pir Pau turning circle. However, the minimum water depth of -1.6 m is observed in the intertidal zone, towards the western side of the creek near the Green Island, while the maximum water depth in the creek records a depth of 6.4 m close to the Trombay channel, with respect to chart datum. The 3D model of the bathymetry of MTC represents an unconventional scenario of undulating seabed depths (Fig. 4b).

## 6.2 Seismic signature of MTC

Considering the fluctuating water depths in the inter-tidal zone of MTC, high resolution shallow seismic acquisition is executed by sectoring the MTC into Sector-1 (western flank of MTC), Sector-2 (middle portion of the MTC) and Sector-3 (eastern flank of MTC). Sector-1 is characterized by highly reflective eastward dipping seabed, but at some places the sea bed shows anomalous irregularity due to dredging activities (Fig. 5). The acoustic basement is discontinuous due to the presence of gas masking zones. High amplitude, continuous and sub-parallel reflectors are evident from the seismic section between seabed and acoustic basement, indicating the presence of consolidated well stratified sedimentary layers.

Though the deepest reflection is recorded at ~15 m (from the seabed) in the western end of the sector-1, the overall sediment thickness varies from 2 m to 10 m. Integration of litho-log information (MMRDA, Technical Report, 2017) reveals that the acoustic basement in sector-1 represents the upper boundary of highly weathered basalt except at the gas masked zone. In sector-2, both the seabed and acoustic basement is characterized by high amplitude continuous reflector. The seabed in central region of the sector-2 shows a syncline pattern with a westward dipping trend, while the acoustic basement information is discontinuous and obscured due to the presence of gas mask zones. Sector-2 shows well defined reflection between the seabed and the acoustic basement on the western side contradicting the vague reflection from its eastern counterpart. This varying reflection patterns reinforce the influence of differential depositional circumstances at MTC. Sector-2 serves as depositional basin for the two prominent creeks involving Thane creek and Panvel creek. The fine-grained sediment supply from the Thane creek represents the mature depositional stage on the western side of sector-2, while the Panvel creek joins the Thane creek on its midway with less sorted, comparatively coarser grain sediments on the eastern side of sector-2. Three prominent gas masking zones have been identified in sector-2, which is classified into Type-1 trapped at deeper depth with trapping layer bulges upward indicating upward forcing of the gas, whereas type-2 is trapped at shallow depth (1-2 m below seabed) with trapping layer follows deposition pattern indicating localized formation of the gas. The sediment thickness varies from least thickness of ~2 m in the western end of the sector to a maximum of ~15 m in the syncline region. The seismic section in sector-3 does not show any gas mask features, but shows a few multiple reflectors. The seabed shows a regular pattern with comparatively shallow acoustic basements. Integration of litho-log information shows that the acoustic basement in sector-3 represents upper boundary of sandy layer. However, the high resolution shallow seismic sections of MTC do not represent any signature of relative displacement of the reflectors between the seabed and acoustic basement, emphasizing that the

seismic section, is devoid of any neo-tectonic activity. The detailed high resolution shallow seismic interpretation of MTC extending up to a depth of ~22m is shown in Figure 5.

### **6.3 Identification of the lineaments**

Different edge detection techniques have been applied to delineate the lineaments/faults in the Thane creek. Solutions from the tilt derivative, Euler deconvolution are merged with the selected crest value of the horizontal derivatives. The lineaments are marked where the location of the cluster solution from tilt derivative and Euler deconvolution are consistent with the horizontal derivative (Fig. 6a). Location of each fault is marked where the linear alignment of all the three solutions are observed. A set of nineteen lineaments trending in north-south direction are identified in the entire study region. Considering the proximal location and continuity in the NE-SW trend of the lineaments from MTC with the Alibagh-Uran fault zone identified on land, we infer the interpreted lineaments/fault zone of MTC as the marine extension of the Alibagh-Uran fault zone (Figs. 6a and b). Based on the geological study performed on land/intertidal zone, Desai and Bertrand (1995) suggested that the Alibagh-Uran as fault zone which is 25 m wide at Alibagh and widens up to 200 m at Uran. However, the width of its marine analogue in MTC is ~900 m (between F7 and F8) wide at the northern side, while on the southern extreme of the Thane creek the width ranges from ~581 m (between F17-F19) to ~710 m (between F17 and F18) encompassing the East and West faults of the Elephanta Island identified by Samant et al. (2017). The N-S trend of the lineaments observed in the Thane creek are coherent with both the Dharwar trend and the early spreading direction between India and Laxmi Ridge, which later changed its spreading direction to east-west. However, the association of the lineaments in the thane creek with these tectonic events is uncertain. Figure 6a represents the estimated contact solutions from horizontal derivative, analytic signal, and tilt angle method. The identified lineaments in MTC are plotted on top of the RTP map of the MTC (Fig. 6b).

### **6.4 Source Depth estimation using Derivative Filters**

Depth to the source is estimated using several depth estimating techniques. SED has shown a depth range from 15 m to 830 m for structural index  $N=0$ . The depth estimated from the zero contour of the TD (Blakely et al. 2016) map records a minimum depth of 35 m and a maximum depth of 900 m. Considering the depth solutions estimated from AS, the minimum depth estimated is 6 m and the maximum depth reaches up to 850 m. The depth estimated from SPI records a minimum depth of 35 m and maximum depth of 902 m. The depth solutions estimated from different methods shows maximum concentration within the depth range of 50 m to 600 m. The total magnetic anomaly of the MTC is influenced by these highly magnetized layers of flood basalt with varying thickness

emplaced in different depth. The lineaments/fault may have deeper extension beyond the maximum depth solutions recorded by the methods and continue to several magnetic layers emplaced in deeper depths. It is difficult to differentiate the comparatively weak magnetized anomalies associated with the lineaments/fault from the highly magnetized basalt flow. This is mainly because the high magnetization of the basalt flow dominates the anomalies associated with the lineament/faults embedded in them. Also, the magnetic anomaly is biased by the thickness and depth of emplacement of the basalt flow layers. All the derivative methods provide a range of the depth solutions, but the density of the solutions decreases with increasing depths. The depth to the source estimated for different derivative methods is shown in Figure 7.

## 7 Discussion

The complex breakup between India and Laxmi-Seychelles, subsequently between India-Laxmi and Seychelles and the associated periodic volcanism by the Reunion hotspot is manifested in MTC as emplacements of flood basalt in different layers, with varying thickness. Hence the total magnetic field intensity recorded is the cumulative effect of all the basalt layers along with the identified lineaments in MTC. The source depth estimated for the lineament/faults is influenced by the presence of the highly magnetized thick basalt flow. For better comprehension of the role of the flow and their influence on the magnetic anomaly caused by the lineaments, it is inevitable to estimate the depth to the top and bottom of the flow. To achieve this, we have performed spectral analysis in MTC. However, the depth to the top and depth to the base of the basalt layer have crucial influence in determining the overall thickness of the basalt flow.

### 7.1 Thickness of the flow layer

The concept of 2D spectral analysis was first introduced by Spector and Grant, 1970 to estimate the depth to the top of the magnetic layer ( $Z_t$ ) from the slope of the log power spectrum. Later Bhattacharyya and Leu (1975 and 1977) developed the method to estimate the centroid of the magnetized layer ( $Z_0$ ). Further Okubo et al. 1985 improved this method to determine the depth to the bottom ( $Z_b$ ) of the magnetized layer. Spector and Grant (1970) proposed the idea of the radial average of the power density spectra considering random and uncorrelated magnetization of two-dimensional bodies. The power density spectra of the total field anomaly

$$F(k) = A_1 e^{-2|k|Z_t} (1 - e^{-2|k|(Z_b - Z_t)})^2 \quad (1)$$

where  $k$  represents the wavenumber,  $Z_t$  is depth to the top of the magnetic layer and  $Z_b$  is the depth to the bottom of the magnetized body and  $A_1$  is a constant.

The centroid depth ( $Z_0$ ) of the magnetized layer is determined from the slope of the longest wavelength divided by the wave number.

$$\ln\left(\frac{F(k) \cdot k^2 / g}{k}\right) = A - k/Z_0 \quad (2)$$

and depth to the top of the magnetized body is determined from the slope of high wavenumber portion of the power spectrum.

$$\ln\left(F(k) \cdot k^2 / g\right) = B - k/Z_c \quad (3)$$

where A and B are constants.

The depth to the base of the magnetic layer is derived by (Okubo et al. 1985; Tanaka et al. 1999) as

$$Z_b = 2Z_0 - Z_c \quad (4)$$

To confine the top and bottom boundary of the source, we have executed spectral analysis considering 18 windows of 2000x2000 m with an overlap of 500 m (Fig. 8). The depth estimated for different windows are shown in the table 1. The radially average power spectrum of window 15 is represented in Figure 9.

The western flank of MTC includes windows W-1, W-2 and W-3. The depth to the top of the magnetic layer varies from 26 m, 56 m and 76 m respectively where the corresponding depth to the bottom is estimated at 510 m, 607 m and 476 m. The average thickness of the magnetic layer is estimated to be ~478 m in the western region of the creek. The central region of MTC includes W-4, W-5, W-6, W-7, W-8, W-9 with depth to the top of the magnetic layer undulating drastically from 54 m, 20 m, 12 m, 70 m, 57 m, 53 m respectively and has corresponding depth to the base of the flow of 528 m, 476 m, 654 m, 635 m, 397 m, and 490 m. The average thickness of the magnetic layer for the central MTC is estimated at 498 m. The windows in the eastern flank comprise W-10, W-11, W-12, W-13, W-14 with depth to the top of magnetic layer estimated at 52 m, 51 m, 18 m, 43 m, 46 m and depth to the base of the magnetic layer of 483m, 509m, 561m, 605m, 440m respectively. The average thickness of the magnetic layer in eastern flank is estimated to be 477 m. The windows from the southern side of MTC include W-15, W-16, W-17 and W-18 with depth to the top of the source estimated to be 58 m, 54 m, 52 m and 47 m, whereas, the depth to the base of the magnetic layer is estimated to be 487 m, 651 m, 658 m and 797 m. The average thickness of the magnetic layer in this region is estimated as 566 m. In general, the thickness of the magnetic layer is inconsistent with maximum thickness at the southern sector of the creek and minimum thickness in the western sector of MTC.

Analyzing each window of MTC, the lowest depth to top of the magnetic layer (DTML) value is 12 m determined from W-6. Contrary, the depth to the base of the magnetic layer (DBML) is high with 654 m, estimating the thickness of 641 m for W-6. The highest DTML value of 70 m is determined for W-7 with the DBML value of 635 m and a thickness of 565 m. W-18 shows a thickness of 750 m with highest DBML of 797 m and DTML value of 47 m. The lowest DBML value of 397 m is estimated for W-8, with DTML value of 57 m and thickness 340 m. The average thickness of the magnetic layer in MTC is estimated to be ~504 m. Grid map of DTML and DBML of MTC is shown in Figure 10.

## **7.2 Thickness and Depth of Basalt Flow- Consequences on Lineaments**

The deepest location of the lineaments from the top of the basalt flow, identified from four different derivative filters in MTC (852 m from AS, 839 m from ED, 586 m from SPI and 902 m from TD) is in agreement with the average thickness of the basalt flow (544 m) estimated from the spectral analysis. This shows that the lineaments/faults are embedded within the basalt flow, but may not be confined to the uppermost basalt flow and may have deeper extensions to the flows beneath. Though, the depth of emplacement and the thickness of the basalt flow ultimately determine the magnetic anomaly values, ideally the topmost basaltic layer has greater influence. Hence, the magnetic anomaly measured could be biased, masking the deeper basaltic emplacements along with the imprints of the lineaments/fault embedded in them. The thickness map of MTC is shown in Figure 11.

Cox and Hawkesworth 1985; Beane et al. 1986; Devey and Lightfoot 1986; Subbarao et al. 1994; Jerram and Widdowson 2005 have performed various geochemical, petrological, stratigraphic, magnetostratigraphic and paleomagnetic analysis on the Deccan continental flood basalt along the western Ghats of India, suggesting three major subgroups from oldest Kalsubai of ~2000 m thick, comparatively younger Lonavala of ~525 m thick and youngest Wai of ~1100 m thick, Furthermore, the subgroups are divided into twelve formations and each formation is differentiated from the other based on the flow type, rock structure and the chemical composition (Najafi et al. 1981; Mahoney et al. 1982; Cox and Hawkesworth 1985; Beane et al. 1986; Devey and Lightfoot 1986; Bodas et al. 1988; Khadri et al. 1999). Delineating the four main formations in the Mumbai region, from top to bottom includes the youngest Khandala formation of 140 m thickness representing the oldest formation from the Lonavala subgroup. Comparatively older formations of Bhisamashankar, Thakurvadi and Neral underlie one another with thickness of 140 m, 650 m and 100 m respectively; comprise the Kalsubai sub-group (Chenet et al. 2008). Considering the proximal location of MTC near Mumbai, one could expect the occurrence of all or the combination of any of the four

formations corresponding to each basalt flow, representing the overall thickness of the basalt flow in MTC. The thickness estimated for the basalt flows from the current study falls within the overall thickness of ~1000 m for the formations. The precise identification of each formation requires detailed geochemical analysis, which is out of the scope of our study; hence the uncertainty in documenting the identity of the formations for the basalt flows in MTC. The Thaakurvadi formation being the thickest basalt flow has the higher probability of occurrence in MTC with the least probability of thin Neral formation beneath. However, the presence of overlying thin formations of Khandala and Bhisamashankar could not be ruled out.

To demonstrate the effect of varying thickness and depth of emplacement of the Deccan basalt flows in MTC, confining the upper 160 m from the mean sea level, a 2D forward model is generated using GM-SYS software (Fig. 12). The model is calibrated using litholog and geologic information from 273 boreholes along ~7 km, with the observed magnetic anomaly of MTC (MMRDA, Technical Report, 2017). Various paleomagnetic studies have been conducted to estimate the age of Deccan flood basalt (e.g. Courtillot et al. 1986; Pande 2002; Hofmann et al. 2000; Chenet et al. 2007) reports a dominating magnetic polarity of C29r (reversal) followed by a short span of C29 normal for the southern region of Deccan flood basalt. The paleomagnetic study by Courtillot et al. 1986 from the northern Narmada valley assert an age of C30 normal for the Deccan flood basalt. Considering the location of the MTC, we have considered single basaltic flow of chron of 29R (~ 66 Ma-65 Ma) outpoured over the pre-faulted zone manifesting the present structural configuration. The top of the basaltic flow is assumed to be extremely weakly susceptible due to high weathering. Observed magnetic data along the profile shows the presence of both high and low amplitude magnetic anomalies. Low amplitude anomalies are interpreted to be due to the variable thickness of flood basalt below the sediment whereas anomalies of high amplitude are generated by the sudden change of depth and thickness in basaltic flow, which can be interpreted as the presence of faults/displacement at places in the flood basalt layer. The high amplitude negative anomaly at some places is justified by the presence of normal polarity intrusive bodies.

### **7.3 Implication of the Lineaments/Faults on tectonic scenario of Mumbai coast**

Mohan et al. 2007, Raghu Kanth and Iyengar, 2007, Gupta et al. 1998, Nandy 1995 discussed the seismic studies along the Konkan region comprising Mumbai region and along the Panvel flexure zone. The observation was conducted from 1998 to 2000 recording an average of 20 events per year and 10 events per year from 2001-2005. About 27 seismic events were recorded in the vicinity of Panvel flexure zone between magnitude (Mw) 2.5 and 2.9. An average of 14 earthquake events for magnitude greater than 3.0 Mw is recorded at a depth of 5 km closer to Panvel, with 3.6 Mw as the

highest magnitude recorded. Considering the depth of hypocenters, earthquakes were categorized into near surface (< 2 km), shallow (2-15 km) and deep (> 15 km) with magnitudes ranging from 2.5-3.3 Mw. Though some of these hypocenters contributed to the historical earthquakes (eg: Chandra et al. 1977, Bansal and Gupta, 1998, the Bombay earthquake of 1618 with intensity IX), none of these hypocenters are located within the boundary of the MTC (Fig. 13). Mohan et al. (2007) suggested that the near surface earthquakes within 2 km basaltic emplacements are probably due to the failure of faults aligned on the flanks of Panvel flexure zone. In the present study, seismic section from the central MTC (Fig. 5b) do not show any apparent signature in dislocation of the sedimentary strata due to faulting up to a depth of ~35 m, rather the seismic section exhibits gas masking features for the inferred Alibagh-Uran fault zone. The gas masking shows convex upward signature which indirectly emphasize the strong seepage of gas from deeper weak zone. The location of gas mask zone identified in the sedimentary strata of the MTC coincides with the extended location of the Alibagh-Uran fault zone. We infer that the Alibagh-Uran fault embedded in the deep-seated flood basalt may act as the weak zone which favored the gas to seep through the sedimentary layers of the MTC to form gas mask zones. The prominent Uran-Dabhol lineament reported from the previous studies (Dessai et al, 1990; Dessai and Bertrand, 1995) crosses the southern part of the Alibagh-Uran Fault zone at ~18° 56'N latitude, and reaches to the western side of the MTC intersecting the lineaments/faults F2-F2', F3-F3' and F4-F4' (Figs. 5a, 6b). It may be noted here that the signature of the Uran-Dabhol lineament is not observed either in the sedimentary strata in the high-resolution seismic section or in the magnetic anomaly map.

The set of lineaments/faults identified in the present study are not exceeding ~600 m of depth, therefore following Mohan et al. (2007) we classify the identified lineaments/faults in the MTC as near surface weak zones embedded in the basaltic layers. Further, Mohan et al. (2007) suggested that the shallow and deep crustal earthquakes are driven by reactivation of basement faults, whereas near surface earthquakes occur within the Deccan Traps due to failure of the faults flanking the Panvel Flexure zone. Widdowson and Mitchell (1999) explained how the deep-seated basement faults rejuvenate and propagate to the top layers of basalt due to isostatic adjustments. Mohan et al. 2007 proposed that the observed seismicity may be due to the regional tectonics and isostatic adjustments. Predominant micro-seismicity associated with the Panvel flexure was reported by Mohan et al. (2007). Though Subrahmanyam (2001) reported seismic activity of magnitude 3.6 on 31<sup>st</sup> May, 1998 with epicenter located in the Panvel creek, the mid-Thane creek of Mumbai did not record any seismicity in the identified near surface weak zones



## 8 Conclusions

An integrated geophysical survey comprising single beam bathymetry, high resolution seismic and magnetic data were conducted in the MTC including the intertidal zone. Analysis and interpretation of the geophysical data provided tectonic features of the mid-Thane creek and thickness of the flood basalt layer. The important conclusions of the study are as follows:

1. In the intertidal zone of the MTC, the depth ranges from 6.4 m to -1.6 m.
2. Several gas mask zones have been identified in MTC, but no neo-tectonic fault is recorded in the sedimentary strata up to ~35 m depth.
3. A set of nineteen north-south trending faults have been identified in the MTC using different edge detecting derivative methods including tilt derivative, standard Euler deconvolution and horizontal derivative.
4. A fault zone identified in the central region of the MTC is inferred as the marine extension of Alibagh-Uran fault zone passing through the mainland of Alibagh and Uran close to the Mumbai city.
5. The width of the fault zone identified in the central MTC is ~900 m (between F7 and F8) at the northern side, while on the southern extreme of the Thane creek the width ranges from ~580 m (between F17 and F19) to ~710 m (between F17 and F18).
6. The depth of the lineaments/faults have been identified using various depth estimating derivative techniques including analytic signal, Euler deconvolution, tilt derivative, source parameter imaging. Though, the depth estimated from the different methods are not consistent, the maximum depth solutions are concentrated within the depth range of 50 m to 600 m.
7. Average thickness of the basalt layer is estimated as ~500 m, with minimum thickness of ~340 m in the central region and maximum thickness of ~750 m in the eastern region of the MTC.
8. The depth of the lineaments/faults are in congruent with the depth and thickness of the flow basalt layer, emphasizing that the lineament/faults are confined within the flood basalt layer.
9. The identified lineaments/faults in the MTC are classified as near surface weak zones embedded in the basaltic layers with no reported occurrence of earthquakes.

## Acknowledgement

The authors are grateful to the Prof. Sunil Kumar Singh, Director, CSIR-National Institute of Oceanography, Goa for the support and permission to publish this work. Sincere thanks to Mumbai Metropolitan Region Development Authority (MMRDA) for approaching Dr. Anil K. Chaubey, Scientist-in-Charge, CSRI-NIO, Regional Center, Mumbai to conduct the geophysical survey under the project no: SSP3170. We acknowledge the instrumentation team and the survey team from CSIR-NIO, Head Quarters, Goa for the excellent technical and field assistance. Seismic processing and interpretation are performed using SeisSpace®ProMAX®. Magnetic data processing, interpretation and integrated modeling are carried out using Geosoft-Oasis Montaj software. Eco-sounder data is processed using HYPACK® software. The support from the survey boat crew is specially mentioned with gratitude. **This is NIO contribution XXXXXXXX.**

## References

- Auden J B 1949 Dykes in western India-a discussion of their relationship with the Deccan Traps; *Trans. Natl. Inst. Sci. India* 3 123-159.
- Bansal B K and Gupta S 1998 A glance through the seismicity of peninsular India; *J. Geol. soc. India*. 52 67-80.
- Barbosa V C F, Silva J B C and Medeiros W E 1999 Stability analysis and improvement of structural index estimation in Euler deconvolution; *Geophysics* 64 48-60.
- Baranov V 1957 A new method for interpretation of aeromagnetic anomalies: Pseudogravimetric anomalies; *Geophysics* 22 359-383.
- Beane J E, Turner C A, Hooper P R, Subbara K V and Walsh J N 1986 Stratigraphy, composition and form of the Deccan basalts, Western Ghats, Deccan, India; *Bull. Volcanol.* 48 61-83.
- Bhattacharyya B K and Leu L 1975 Analysis of magnetic anomalies over Yellowstone National Park, Mapping the Curie-point isotherm surface for geothermal reconnaissance; *J. Geophys. Res.* 80 461-465.
- Bhattacharyya B K and Leu L 1977 Spectral Analysis of Gravity and Magnetic Anomalies due to Rectangular Prismatic Bodies; *Geophysics* 42 41-50.
- Bhattacharya G C and Yatheesh V 2015 Plate-tectonic evolution of the deep ocean basins adjoining the western continental margin of India e a proposed model for the early opening scenario. In: Mukherjee, S. (Ed.); *Petroleum Geosciences: Indian Contexts, Springer Geology* 1-61.
- Biswas S K 1982 Rift basins in western margin of India and their hydrocarbon prospects with special reference to Kutch basin; *Bull. Assoc. Petrol. Geol.* 66 1497-1513.

Biswas S K 1987 Regional tectonic framework, structure and evolution of the western marginal basins of India; *Tectonophysics* 135 307-327.

Blakely R J, Connard G G and Curto J B 2016 Tilt Derivative Made Easy; Geosoft, U.S. Geological Survey, Menlo Park, California. [www.geosoft.com/resources/goto/tilt-derivative-made-easy](http://www.geosoft.com/resources/goto/tilt-derivative-made-easy)

Bodas M S, Khadri S F R and Subbarao K V 1988 Stratigraphy of the Jawhar and Igatpuri formations, Western Ghats lava pile, India, in Deccan Flood Basalts, edited by Subbaro K. V, *Mem. Geol. Soc. India* 10 235-252.

Chandra U 1977 Earthquakes of peninsular India -A seismotectonic study; *Bull. Seismol. soc. America* 67 1387-1413.

Chandrasekharam D 1985 Structure and evolution of the western continental margin of India deduced from gravity, seismic, geomagnetic and geochronological studies; *Phys. of the Earth and Planet. Inter.* 41 186-198.

Chenet A L, Quidelleur X, Fluteau F and Courtillot V 2007  $^{40}\text{K}$ - $^{40}\text{Ar}$  dating of the main Deccan large igneous province: Further evidence of KTB age and short duration; *Earth Planet. Sci. Lett.* 263 1-15.

Chenet A L, Fluteau F, Courtillot V, Gérard M. and Subbarao K V 2008 Determination of rapid Deccan eruptions across the Cretaceous-Tertiary boundary using paleomagnetic secular variation: Results from a 1200-m-thick section in the Mahabaleshwar escarpment; *J. Geophys. Res.* 113 B04101.

Choudhary B R and Jadhav G N 2014 Petrogenesis of fractionated basaltic lava flows of Poladpur-Mahabaleshwar formation around Mahabaleshwar, Western Ghats, India, *J. of the Geol. Soc. of India* 84 2 197-208.

Courtillot V, Besse J, Vandamme D, Montigny R, Jaeger J.-J and Cappetta H 1986 Deccan flood basalts at the Cretaceous/Tertiary boundary?; *Earth Planet. Sci. Lett.* 80 361-374.

Cox K G and Hawkesworth C J 1985 Geochemical stratigraphy of the Deccan Traps at Mahabaleshwar, Western Ghats, India, with implications for open system magmatic processes, *J. Petrol.* 26 355-377.

Dessai A G, Rock N M S, Griffin B J and Gupta D 1990 Mineralogy and petrology of xenolith-bearing alkaline dykes associated with Deccan magmatism, south of Bombay, India; *Eu. J. Mineral.* 2 667-685.

Dessai A G and Bertrand H 1995 The 'Panvel Flexure' along the western Indian continental margin: An extensional fault structure related to Deccan magmatism; *Tectonophysics.* 241 165-178.

Devey C W and P C Lightfoot 1986 Volcanological and tectonic control of stratigraphy and structure in the western Deccan Traps; *Bull. Volcanol.* 48 195-207.

Duncan R A and Pyle D G 1988 Rapid eruption of the Deccan flood basalts at the Cretaceous/Tertiary boundary; *Nature* 333 841-843.

Fernandes L, Nayak G N and Ilangovan D 2012 Geochemical Assessment of Metal Concentrations in Mangrove Sediments along Mumbai Coast, India, World Academy of Science, Engineering and Technology; *Int. J. Geolo. and Envir. Engi.* 6 1.

Ghodke S S 1978 Geology of the area around Panvel, Kolaba dist., Maharashtra; *Unpubl. PhD thesis*, University of Pune.

Gombos A, Powell G W and Norton O I 1995 The tectonic evolution of Western India and its impact on hydrocarbon occurrences an overview; *Sediment. Geol.*, 96 1-2: 119-129.

Gupta S, Mohandas V and Lakshman S 1998 Earthquake in Thane Kharghar (Panvel) belt on 31 May 1998; *In Proceedings of the 11th Symposium on Earthquake Engineering, Roorkee*, 17-19.

Hofmann C, Fe'raud G and Courtillot V 2000  $^{40}\text{Ar}/^{39}\text{Ar}$  dating of mineral separates and whole rocks from the Western Ghats lava pile: Further constraints on duration and age of the Deccan Traps; *Earth Planet. Sci. Lett.* 180 13-27.

Jerram D A and Widdowson M 2005 The anatomy of Continental Flood Basalt Provinces: Geological constraints on the processes and products of flood volcanism; *Lithos* 79 385-405.

Khadri S F R, Walsh J N and Subbarao K V 1999 Chemical and magneto-stratigraphy of Malwa Traps around Mognaba region, Dhar District (M. P.); *Mem. Geol. Soc. India.* 43 203-218.

Krishna K S, Rao D G, Murty G P S, Ramana Y V 1989 Sound velocity, density, and related properties along a transect across the Bay of Bengal; *Geo-Marine Letters* 9 95-102.

Kumar P and A K Chaubey 2019 Extension of flood basalt on the northwestern continental margin of India. *J. Earth. Syst. Sci.* 128:81.

Kumar P, Mishra A, Pitchika V K, Kumar S, Dubey K M, Singh D and Chaubey A K 2019 Integrated geophysical appraisal of crustal structure and tectonic evolution of the Angria Bank, western continental margin of India; *Mar. Geophy. Res.* 40 433-449.

Lightfoot P, Hawkesworth C and Sethna S 1987 Petrogenesis of rhyolites and trachytes from the Deccan Trap: Sr, Nd and Pb isotope and trace element evidence; *Contrib. to Miner. and Petro.* 95(1) 44-54.

Mahoney J J, MacDougall J D, Lugmair G W, Murali A V, Sankardas M and Gopalan K 1982 Origin of the Deccan Trap flows at Mahabaleshwar inferred from Nd and Sr isotopic and chemical evidence; *Earth Planet. Sci. Lett.*, 60, 47-60.

Mohan G, Surve G and Tiwari P K 2007 Seismic evidences of faulting beneath the Panvel flexure; *Current Sci.*, 93 991-996.

Miller H G and Singh V 1994 Potential tilt-A new concept for location of potential field sources; *J. of Appl. Geophy.*, 32(2):213-217.

Mukherjee S, Misra A A, Calvès G and Nemčok M 2017 Tectonics of the Deccan Large Igneous Province: an introduction; *Geol. Soc. London, Spec. Publi.* 445 1-9 7.

Mumbai Metropolitan Region Development Authority (MMRDA) 2017 Geotechnical Investigation Report -Revision (1), Mumbai Trans harbor Link Project (Personal communication).

Nabighian M N 1972 The Analytic Signal of Two-Dimensional Magnetic Bodies with Polygonal Cross-Section: Its Properties and Use for Automated Anomaly Interpretation; *Geophysics* 37 507-517.

Najafi S J, Cox K G and Sukheswala R N 1981 Geology and geochemistry of the basalt flows (Deccan Traps) of the Mahad-Mahabaleshwar section, India, in Deccan Volcanism and Related Provinces in Other Parts of the World, edited by K. V. Subbarao and Sukheswala R N *Mem. Geol. Soc. India* 3 300-315.

Nandy D R 1995 Neotectonism and Seismic Hazards in India. *Indian J. Geol.* 67 34-48.

Okubo Y, Graf R J, Hansen R O, Ogawa K and Tsu H 1985 Curie point depths of the island of Kyushu and surrounding areas, Japan; *Geophysics* 50 481- 494.

Owen H G 1976 Continental displacement and expansion of the Earth during Mesozoic and Cenozoic; *Philos. Trans. Soc. London* 281 223-291.

Pande K 2002 Age and duration of the Deccan Traps, India: A review of radiometric and paleomagnetic constraints; *Proc. Indian Acad. Sci.* 111 115-123.

Phillips J D 1998 Processing and Interpretation of Aeromagnetic Data for the Santa Cruz Basin Patahonia Mountains Area, South-Central Arizona: U.S; *Geolo. Surv. Open-File Report* 02-98.

Quadros G, Sukumaran S and Athalye R P 2009 Impact of the changing ecology on intertidal polychaetes in an anthropogenically stressed tropical creek, India, *Aquatic Ecology*, 43(4) 977-985.

Raghu Kanth, S T G and Iyengar R N 2006 Seismic hazard estimation for Mumbai city *Current Sci.* 91 1486-1494.

Mita Rajaram, Anand S P, Erram V C and Shinde B N 2016 Insight into the structures below the Deccan Trap-covered region of Maharashtra, India from geopotential data, From: Mukherjee, S., Misra, A. A., Calve's, G. & Nemcok, M. (eds) *Tectonics of the Deccan Large Igneous Province*. Geological Society, London, Special Publications, 445, <http://doi.org/10.1144/SP445.8>

Ram A, Rokade M A, Zingde M D and Borole D V 2009 Post-depositional memory record of mercury in sediment near the effluent disposal site of a chlor-alkali plant in Thane Creek-Mumbai Harbour, India; *Envi. Tech.*, 30 (8) 765-783.

Reid A B, Allsop J M, Granser H, Millett A J and Somerton I W 1990 Magnetic interpretation in three dimensions using Euler deconvolution; *Geophysics* 55 80-91.

Roest W R, Verhoef J and Pilkington M 1992 Magnetic interpretation using the 3-D analytic signal; *Geophysics* 57(1) 116-125.

Salem A, Williams S, Fairhead J D, Ravat D and Smith R 2007 Tilt-depth method: A simple depth estimation method using firstorder magnetic derivatives; *The Leading Edge* 26 1502–1505.

Samant H, Pundalik A, D'souza J, Sheth H, Lobo K C, D'souza K and Patel V 2017 Geology of the Elephanta Island fault zone, western Indian rifted margin, and its significance for understanding the Panvel flexure; *J. of Earth Syst. Sci.* 126 (1) 9

Sethna G F 1999 Geology of Mumbai and surrounding areas and its position in the Deccan Traps stratigraphy, *J. Geol. Soc. India* 53 359-365.

Sheth H C and Chandrasekharam D 1997a Plume-rift interaction in the Deccan volcanic province; *Phys. of the Earth and Planetary Interi.* 99 3-4 179-187.

Sheth H C and Chandrasekharam D 1997b Early alkaline magmatism in the Deccan Traps: implications for plume incubation and lithospheric rifting; *Phy. of the Earth and Planetary Interi.* 104 4 369-374.

Sheth H C 1998 A reappraisal of the coastal Panvel flexure, Deccan Traps, as a listric-fault-controlled reverse drag structure; *Tectonophysics* 294 143-149.

Sheth H C and Pande K 2014 Geological and <sup>40</sup>Ar/<sup>39</sup>Ar age constraints on late-stage Deccan rhyolitic volcanism, inter-volcanic sedimentation, and the Panvel flexure from the Dongri area, Mumbai; In: Flood basalts of Asia (eds) Sheth H C and Vanderkluyzen L, *J. Asian Earth Sci.* 84 167-175.

Sheth H C and Samanth H 2016 Field Guide to Elephanta Island, Mumbai harbour, India (ACROFI VI, 29/11/16)

Spector A and Grant F S 1970 Statistical models for interpreting aeromagnetic data; *Geophysics* 35 293-302.

Srinivasan V 2002 Post-Deccan Trap faulting in Raigad and Thane districts of Maharashtra; *J. Geol. Soc. India.* 59 23-31.

Stavrev P 1997 Euler deconvolution using differential similarity transformations of gravity or magnetic anomalies; *Geophy. Prosp.*, 45 (2) 207-246.

Subbarao K V, Chandrasekharam D, Navaneethakrishnan P and Hooper P R 1994 Stratigraphy and Structure of Parts of the Central Deccan Basalt Province: Eruptive Models; In: Subbarao, K.V., (Ed.) *Volcanism Wiley New Delhi* 321-332

Subrahmanyam V 2001 Seismic signatures in the Kalu River Basin, Thane district and Mumbai. In *Research Highlights in Earth System Science; Indian Geol. Cong.* 201-204.

Takin M 1966 An interpretation of the positive gravity anomaly over Bombay on the west coast of India; *Geophys. J. Royal Astron. Soc.* 11 527-537

Talwani P 1999 Fault geometry and earthquakes in continental interiors; *Tectonophysics* 305 371-379.

Tanaka A, Okubo y and Matsubayashi O 1999 Curie point depth based on spectrum analysis of the magnetic anomaly data in East and Southeast Asia; *Tectonophysics* 306 461-470.

Thomson D T 1982 EULDPTH: A new technique for making computer-assisted depth estimates from magnetic data; *Geophysics* 47 31–37.

Thurston J B and R S Smith 1997 Automatic conversion of magnetic data to depth, dip, and susceptibility contrast using the SPI™ method; *Geophysics* 62 (3) 807-813.

Verduzco B, Fairhead J D, Green C M and MacKenzie C 2004 New insights into magnetic derivatives for structural mapping; *The Leading Edge* 23 116-119.

Watts A B and Cox K G 1989 The Deccan Traps: an interpretation in terms of progressive lithospheric flexure in response to a migrating load; *Earth Planet. Sci. Lett.* 93 85-97.

Widdowson M and Mitchell C 1999 Large scale stratigraphical, structural and geomorphological constraints for earthquakes in the southern Deccan traps, India: The case of denudationally driven seismicity. In Deccan Volcanic Province (ed. K. V. Subbarao), *Mem. Geol. soc. India* 43 425-452.

Wynne A B 1886 On the geology of the island of Bombay; *Mem. Geol. Surv. India* 2 174-227.

**Table 1:** Depth to top, depth to the centroid, depth to the base and the thickness of the basaltic flow layer in respective windows of the MTC. The longitude and latitude of each window is located tentatively, considering the center of the window, to estimate the thickness of flood basalt layer in the MTC.

<i>Window</i>	<i>Longitude</i> (°)	<i>Latitude</i> (°)	<i>depth to</i> <i>top</i> (m)	<i>Depth to</i> <i>centroid</i> (m)	<i>Depth to</i> <i>base</i> (m)	<i>Thickness</i> (m)
1	72.87697	18.98938	26.927	268.583	510.239	483.312
2	72.89173	18.98182	56.465	332.038	607.611	551.146
3	72.91034	18.98073	76.242	276.515	476.788	400.546
4	72.92436	18.99449	54.904	291.799	528.694	473.790
5	72.92461	18.98089	20.462	363.822	476.788	483.312
6	72.9386	18.99685	12.914	333.806	654.697	641.783
7	72.9388	18.98328	70.048	352.866	635.685	565.637
8	72.95285	18.99701	57.420	227.675	397.929	340.509
9	72.95301	18.98346	53.360	271.879	490.398	483.312
10	72.96709	18.99719	52.213	267.898	483.583	431.369
11	72.96725	18.98364	51.162	280.191	509.220	458.057
12	72.98136	18.99735	18.710	290.287	561.863	543.153
13	72.98147	18.98383	43.885	324.904	605.924	562.038
14	72.99565	18.98847	46.465	243.535	440.605	394.140
15	72.91069	18.94428	58.455	272.898	487.341	428.885
16	72.91094	18.93108	54.331	353.089	651.847	483.312
17	72.92498	18.94476	52.914	355.541	658.169	605.255
18	72.92517	18.93121	47.611	422.611	797.611	750.000



## List of Figures

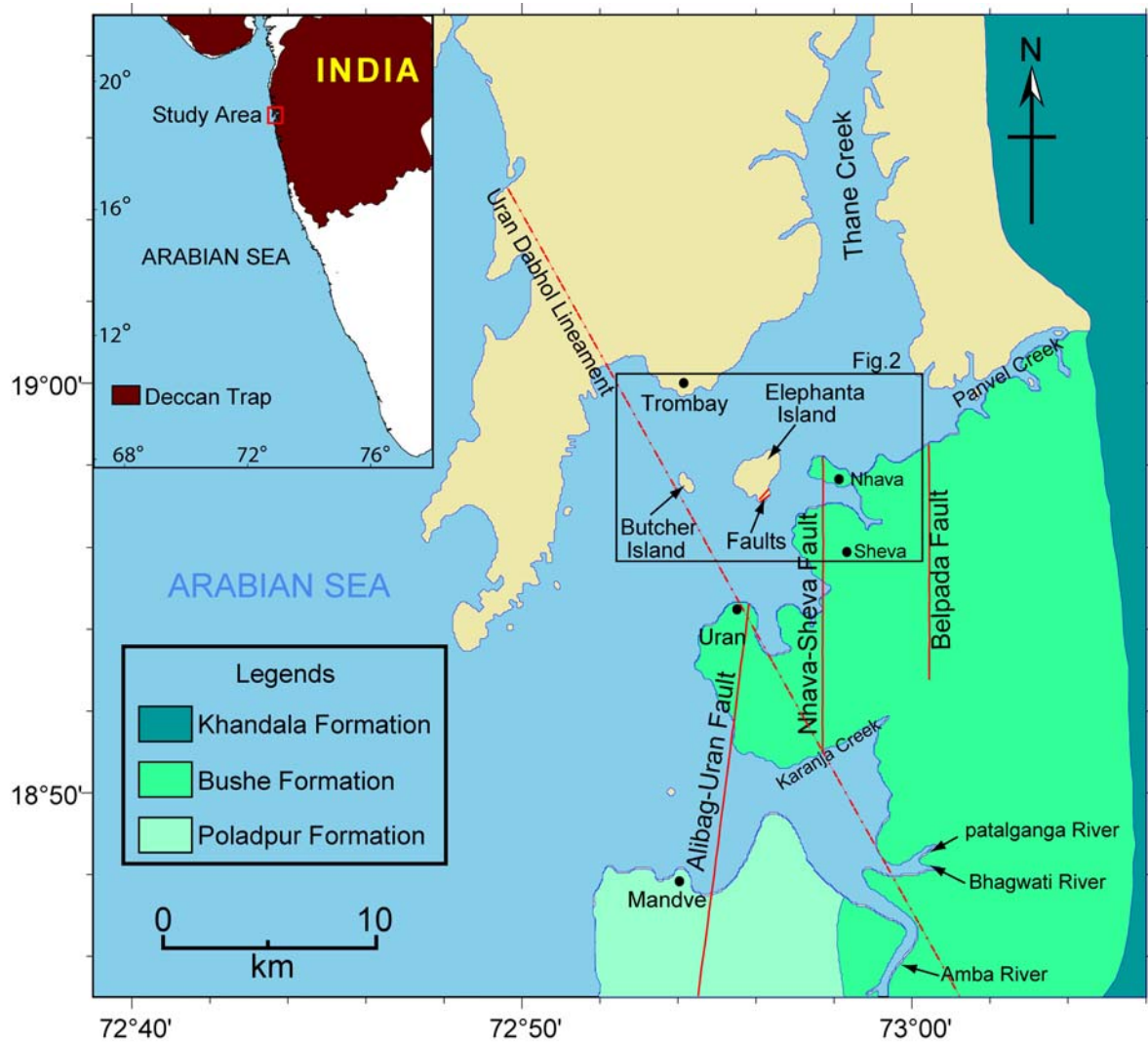
Figure 1	The detailed tectonic and geologic map of the Thane creek. Different colors represent the geologic formations. Inset picture depicts the west coast of India with study area highlighted in red square region. Lineaments and faults are digitized from Dessai and Bertrand (1995); Mohan et al, 2007; Samanth et al., 2017. Rectangular box in black color indicates portion of the map shown in Figure 2.
Figure 2	High resolution shallow seismic survey was limited along 7 track lines with 20 m track spacing along with the echo-sounding, within the central corridor of MTC represented by blue, red and green regions for sector-1, 2 and 3, respectively. Black lines represent the magnetic data acquisition track line synchronized with the single beam bathymetry track lines. Brown lines represent the location of Uran-Dabhol lineament, Nhava-Seva fault, West fault and East fault interpreted in previous studies (Ghodke 1978, Dessai et al, 1990; Dessai and Bertrand, 1995; Samanth et al., 2017).
Figure 3	(a) Total magnetic intensity map of the MTC, (b) Magnetic anomaly map of the MTC reduced to the pole. The plus sign indicates the tentative central location of the spectral windows. Line AB represents the profile chosen for forward modeling of magnetic anomaly data.
Figure 4	(a) The bathymetry profile map along the east-west direction of Mid-Thane creek derived from single beam echo-sounder.  (b) 3D map of bathymetry of Mid-Thane Cree derived from the single beam eco-sounding data integrated with the bathymetry charts from National Hydrographic Office of India.

Figure 5	High resolution shallow seismic sections across the MTC spanning (a) Sector-1 (western part of the MTC) with identified gas mask zones, (b) Sector-2 (central region of the MTC) with identified off-shore extension of Alibagh-Uran Fault/Lineament zone, and (c) Sector-3 (eastern part of the MTC). The acoustic basement is demarked with green solid line.
Figure 6	(a) Solutions derived for delimiting the lineaments/faults using Euler's Deconvolution (SI=0), Tilt angle derivative and the crest of Horizontal derivative, (b) interpreted lineaments/faults superimposed on the RTP map of the MTC. Black lines represent the possible location of lineaments/faults
Figure 7	Depth to the source estimated from (a) Analytical Signal, (b) Tilt Angle, (c) Euler Deconvolution, and (d) Source parameter imaging.
Figure 8	The location and dimension of the spectral windows executed to confine the top and bottom boundaries of the magnetic source (flood basalt layer). We have considered 18 windows of 2000x2000 m with an overlap of 500 m. Window boundaries are represented in black squares and the plus '+' sign represents the tentative center location of each window.
Figure 9	Radially averaged power spectrum for window 15 to estimate (a) depth to the base ( $Z_b$ ) of the basaltic flow, (b) depth to the top ( $Z_t$ ) of the basaltic flow.
Figure 10	(a) Map depicting the depth to the top of the flood basalt layer, (b) depth to the base of the flood basalt layer.
Figure 11	Thickness map estimated for the basalt flow in MTC derived from the 'depth to the top' and 'depth to the base' of the basalt flow layer.
Figure 12	2D forward crustal model of the MTC reaching up to 100 m depth from the mean sea level. The location of interpreted magnetic anomaly profile is

	<p>shown in Figure 3b. Magnetic parameters of flood basalt and intrusive bodies for magnetic anomaly computations are taken as susceptibility 0.0017 CGS unit and remnant magnetization 0.002-0.003 emu/cm<sup>3</sup>. For normally magnetized bodies (pink color intrusive bodies), inclination is -50° and declination is -40° (Kumar et al., 2019).</p>
Figure 13	<p>The west coast of India with the MTC represented in square box. Blue stars represent earthquake hypocenter less than 15 km and green star represents hypocenter greater than 15 km (Mohan et al., 2007). 1- Alibagh-Uran Fault, 2- Nahava-Sheva Fault, 3- Belpada Fault, 4- Panvel Flexure, 5- Uran-Dabhol Lineament (Ghodke 1978; Dessai et al., 1990; Dessai and Bertrand, 1995; Samanth et al., 2017); 6- red colure shaded region represents the marine extension of Alibagh-Uran fault zone interpreted from this study.</p>

### List of Table

Table 1	<p>Shows the depth to top, depth to the centroid, depth to the base and the thickness of the flow layers in respective windows of MTC. The longitude and latitude of each window is located tentatively, considering the center of the window, to estimate the thickness value of MTC.</p>
---------	--



**Figure 1:** The detailed tectonic and geologic map of the Thane creek. Different colors represent the geologic formations. Inset picture depicts the west coast of India with study area highlighted in red square region. Lineaments and faults are digitized from Dessai and Bertrand (1995); Mohan et al, 2007; Samanth et al., 2017. Rectangular box in black color indicates portion of the map shown in Figure 2.

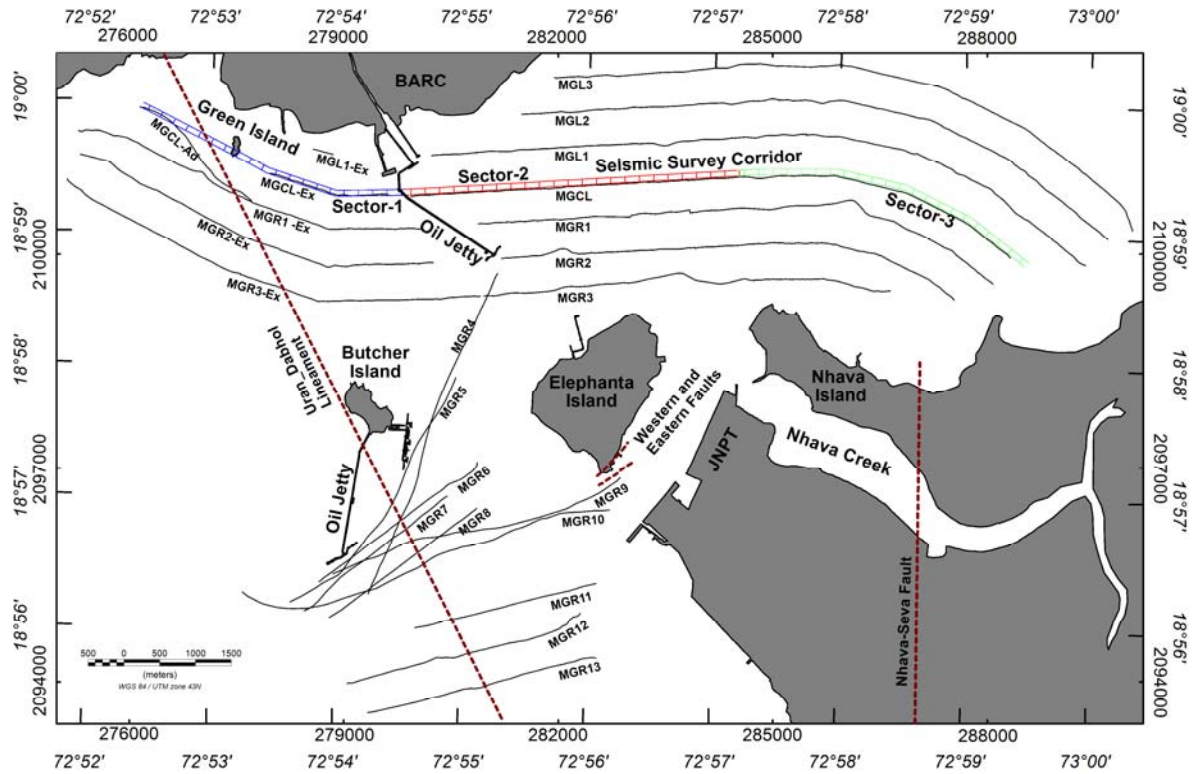


**Figure 2:** High resolution shallow seismic survey was limited along 7 track lines with 20 m track spacing along with the echo-sounding, within the central corridor of MTC represented by blue, red and green regions for sector-1, 2 and 3, respectively. Black lines represent the magnetic data acquisition track line synchronized with the single beam bathymetry track lines. Brown lines represent the location of Uran-Dabhol lineament, Nhava-Seva fault, West fault and East fault interpreted in previous studies (Ghodke 1978, Dessai et al, 1990; Dessai and Bertrand, 1995; Samanth et al., 2017).

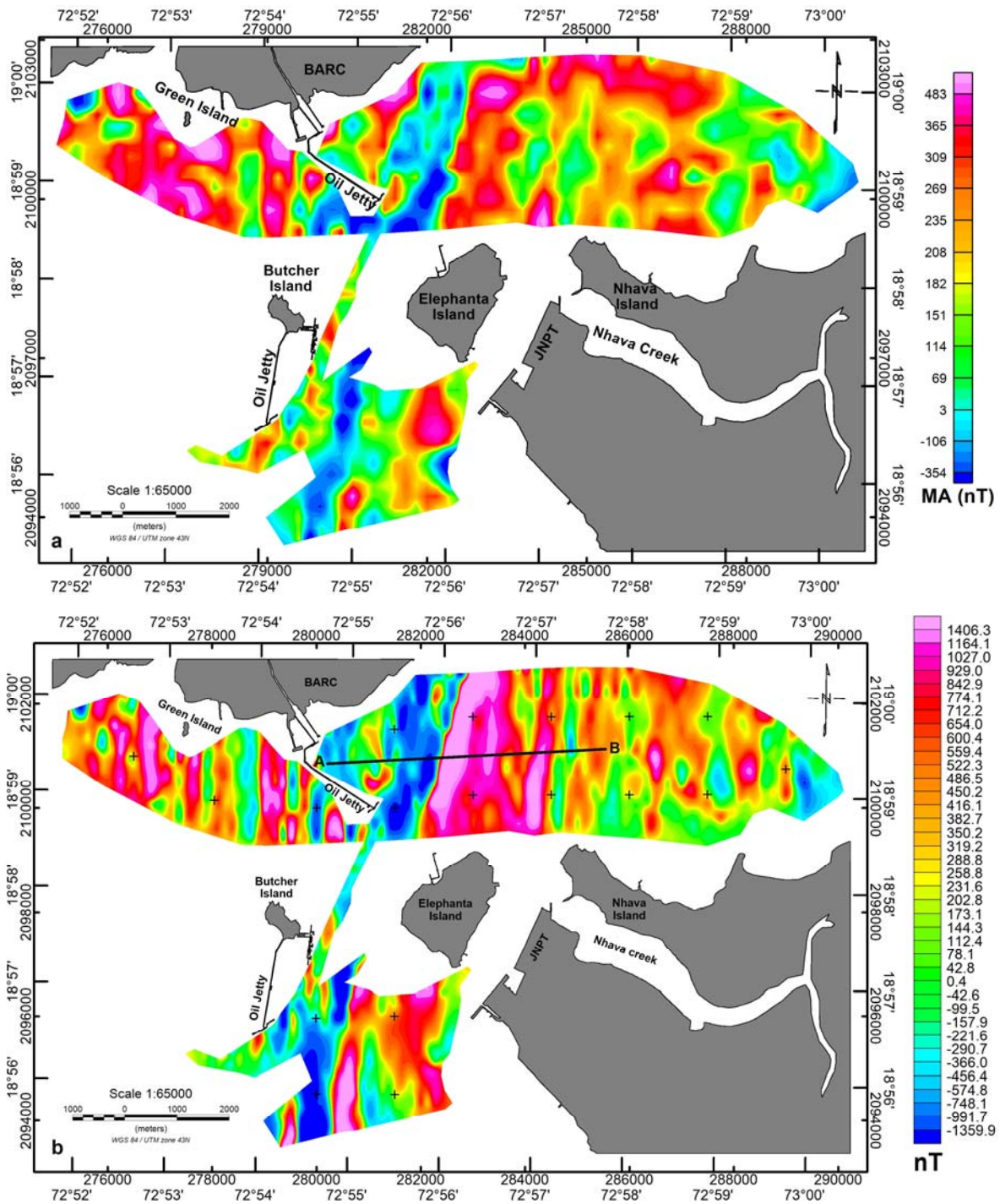


**Figure 3:** (a) Total magnetic intensity map of the MTC, (b) Magnetic anomaly map of the MTC reduced to the pole. The plus sign indicates the tentative central location of the spectral windows. Line AB represents the profile chosen for forward modeling of magnetic anomaly data.



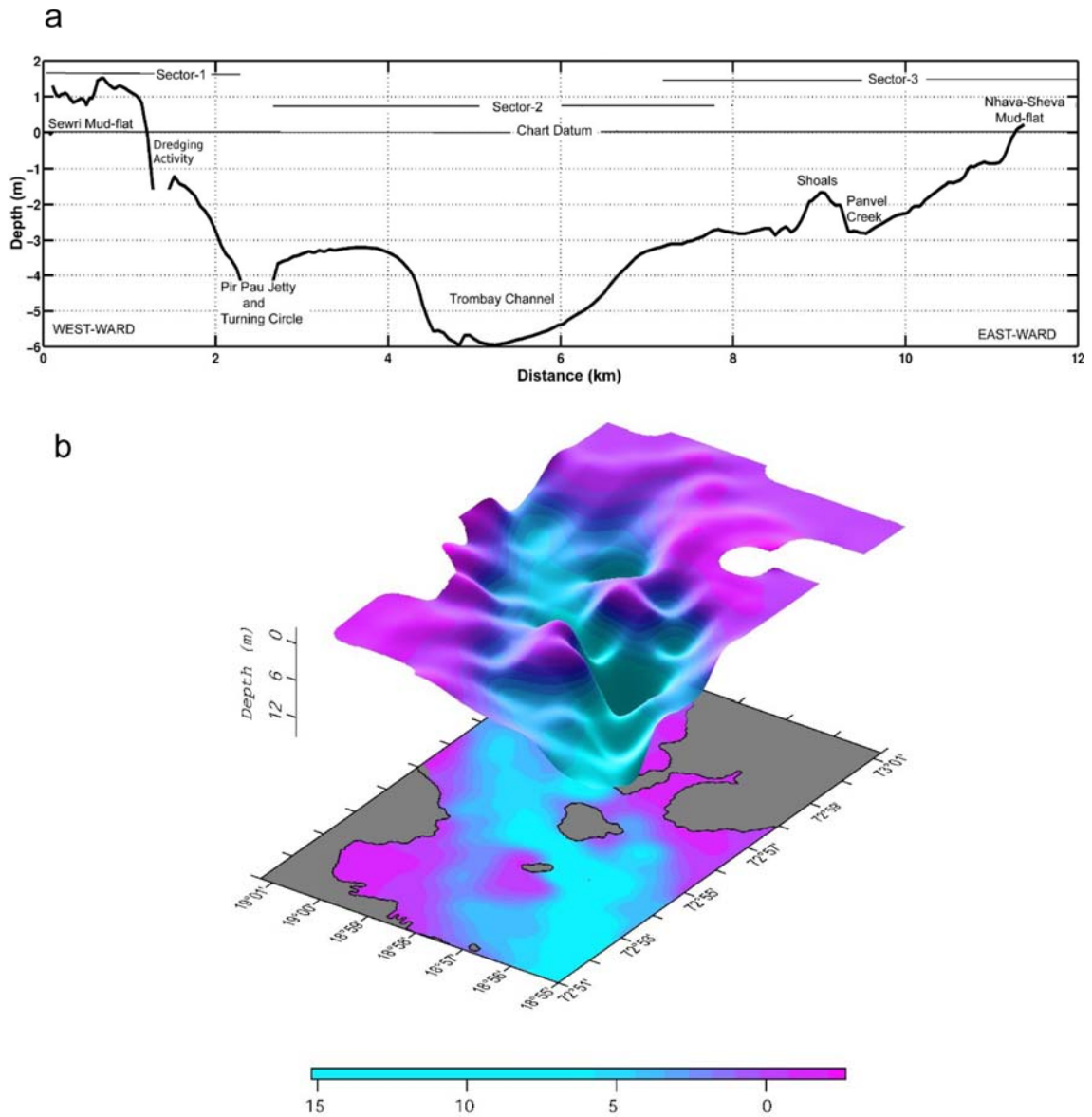


**Figure 4:** (a) The bathymetry profile along the east-west direction in the Mid-Thane creek derived from single beam echo-sounder. (b) 3D bathymetry map of the Mid-Thane creek derived from the single beam eco-sounding data integrated with the bathymetry charts from National Hydrographic Office of India.

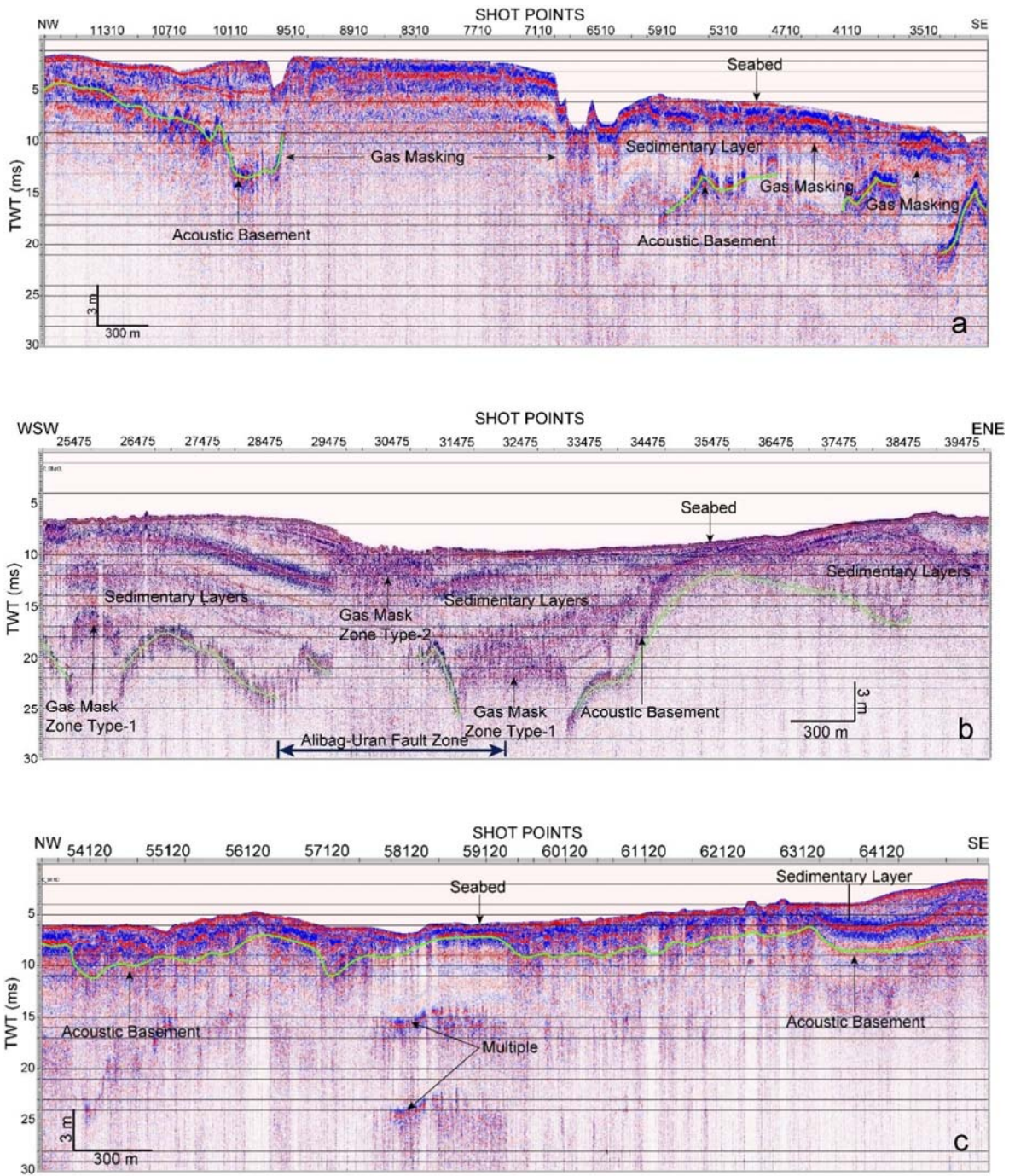


**Figure 5:** High resolution shallow seismic sections across the MTC spanning (a) Sector-1 (western part of the MTC) with identified gas mask zones, (b) Sector-2 (central region of the MTC) with identified off-shore extension of Alibagh-Uran Fault/Lineament zone, and (c) Sector-3 (eastern part of the MTC). The acoustic basement is demarked with green solid line.



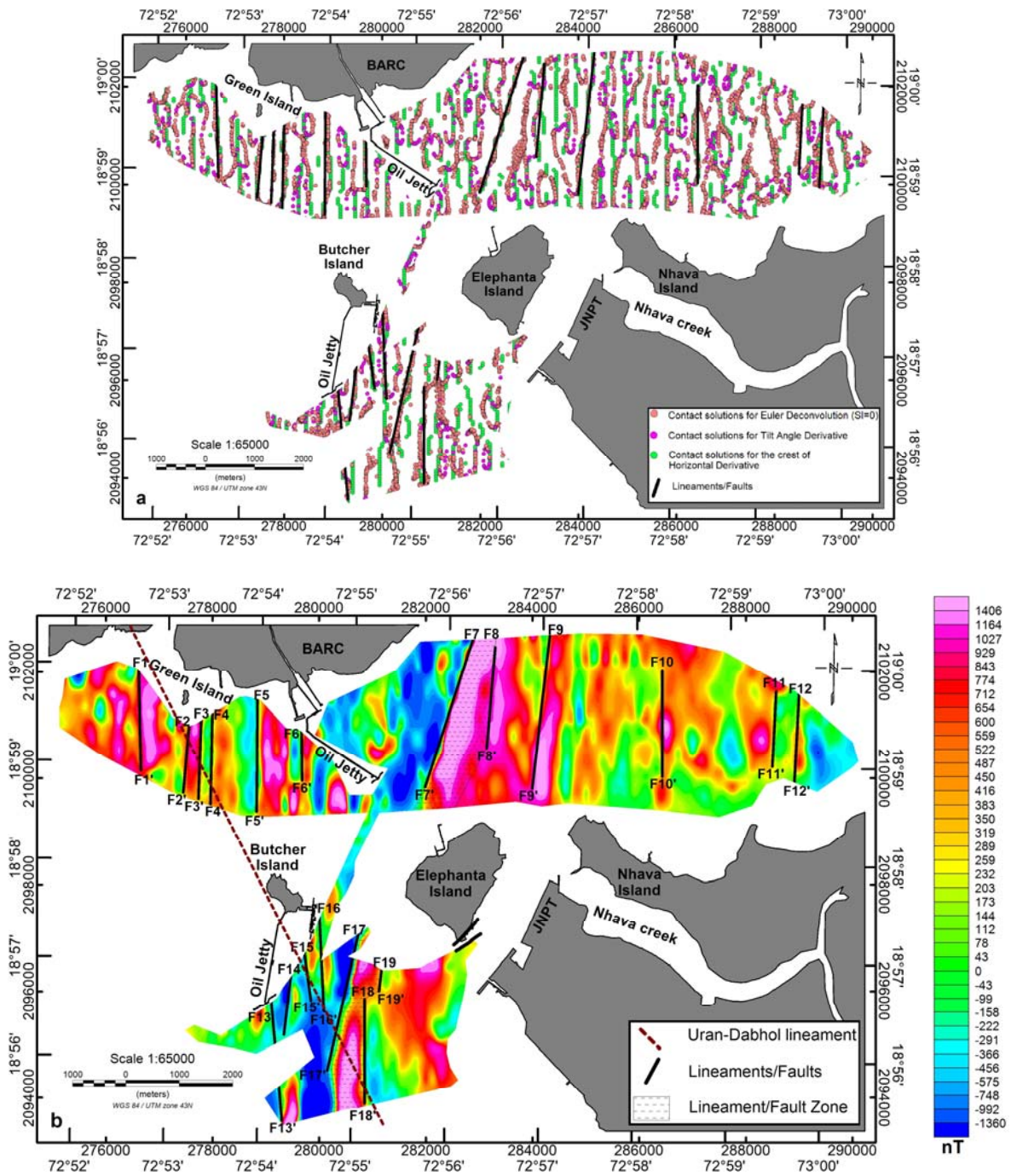


**Figure 6:** (a) Solutions derived for delimiting the lineaments/faults using Euler's Deconvolution (SI=0), Tilt angle derivative and the crest of Horizontal derivative, (b) interpreted lineaments/faults superimposed on the RTP map of the MTC. Black lines represent the possible location of lineaments/faults

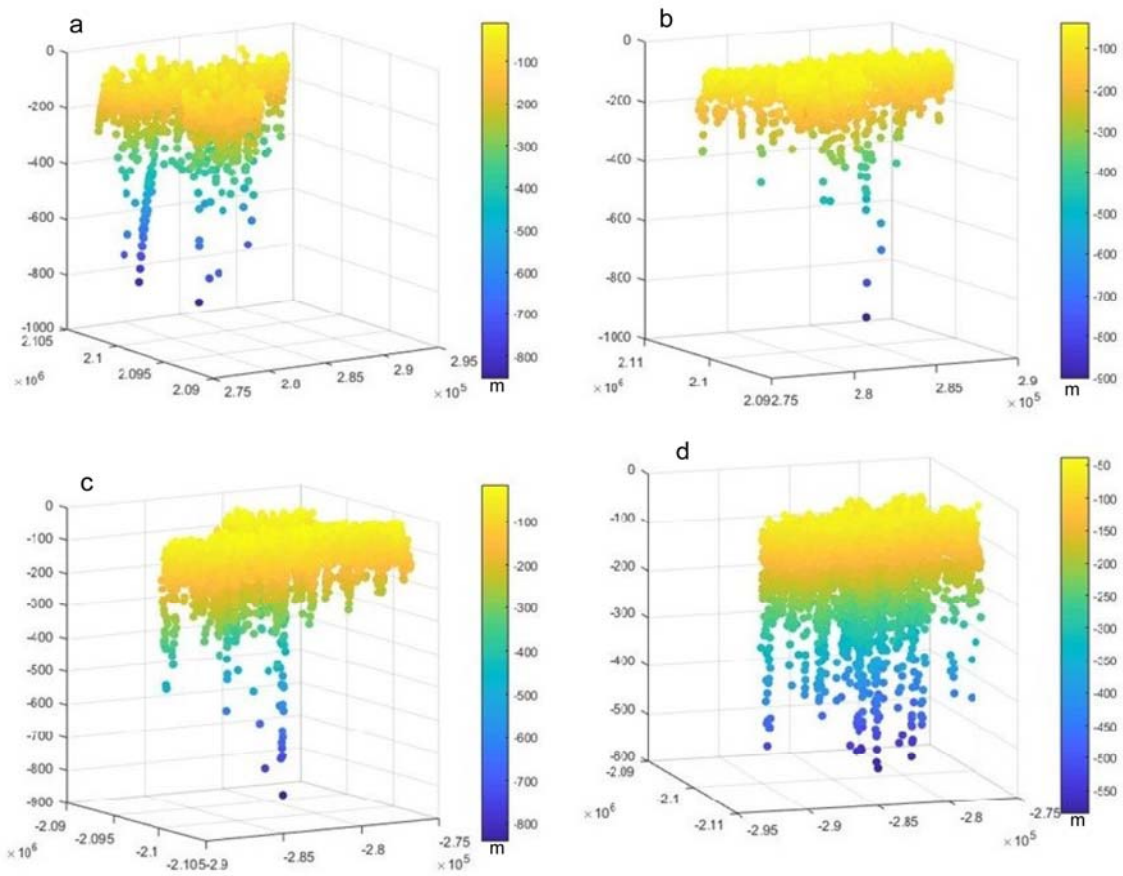


**Figure 7:** Depth to the source estimated from (a) Analytical Signal, (b) Tilt Angle, (c) Euler Deconvolution, and (d) Source parameter imaging.

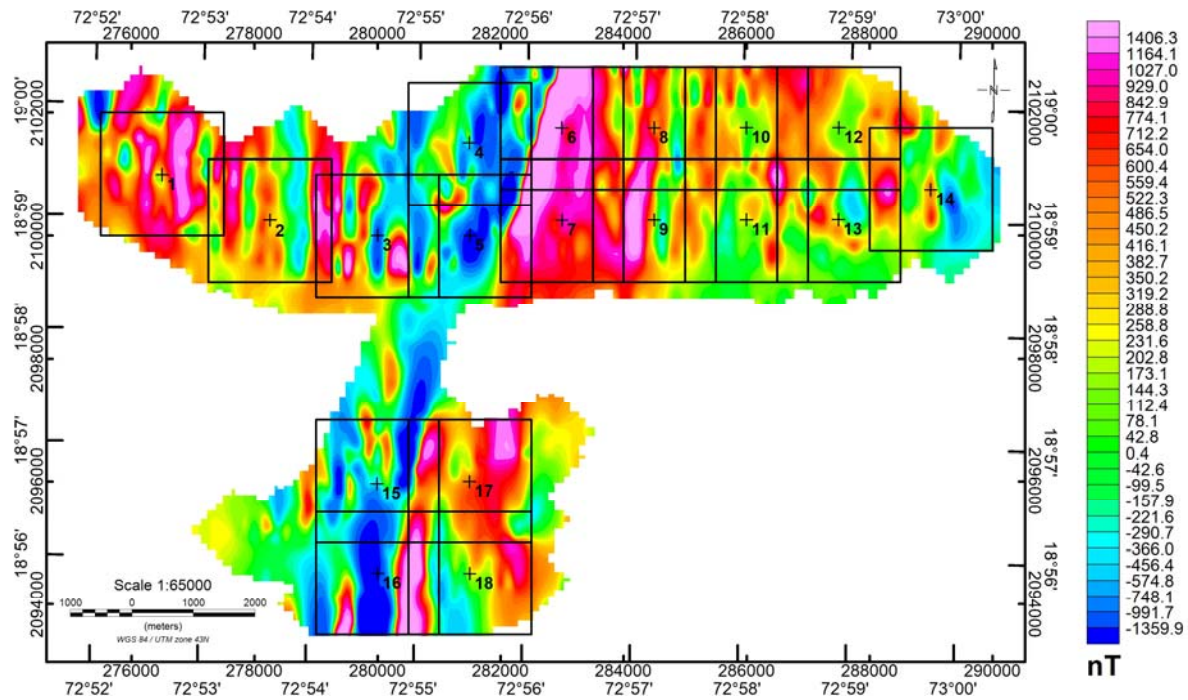


**Figure 8:** The location and dimension of the spectral windows executed to confine the top and bottom boundaries of the magnetic source (flood basalt layer). We have considered 18 windows of 2000x2000 m with an overlap of 500 m. Window boundaries are represented in black squares and the plus '+' sign represents the tentative center location of each window.

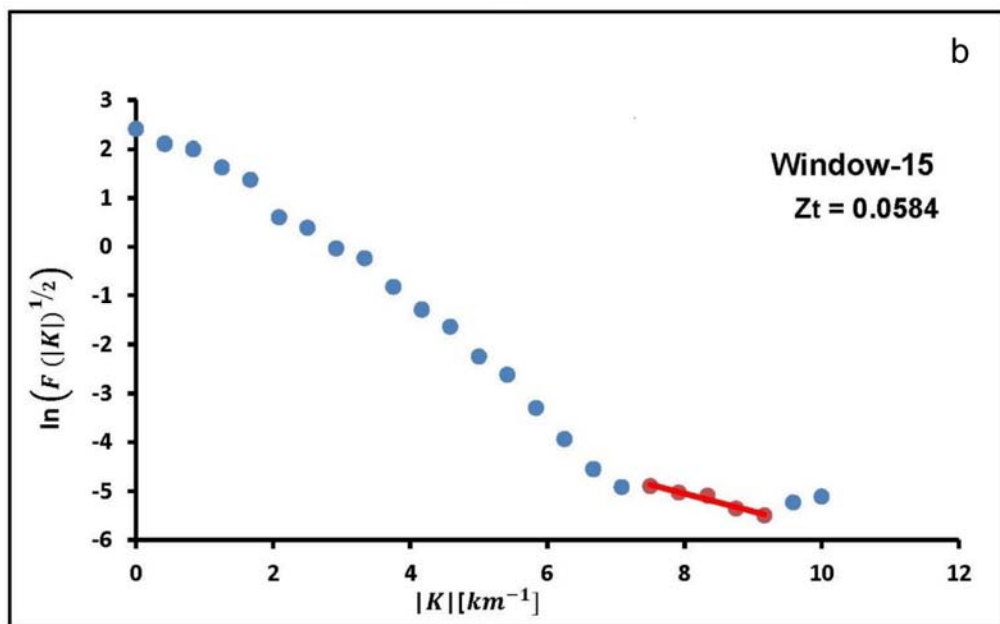
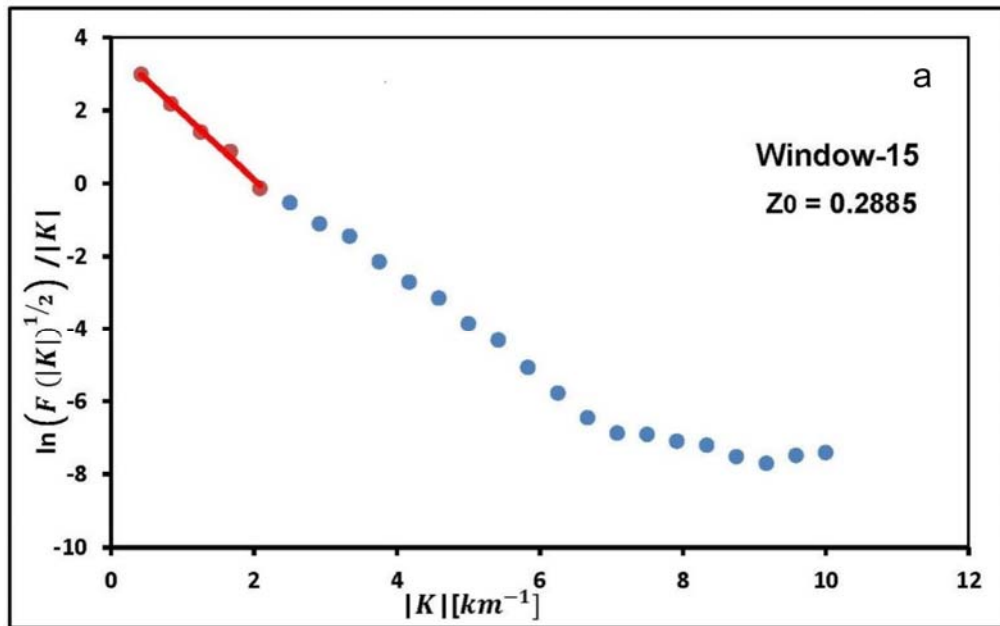


**Figure 9:** Radially averaged power spectrum for window 15 to estimate (a) depth to the base ( $Z_0$ ) of the basaltic flow, (b) depth to the top ( $Z_t$ ) of the basaltic flow.



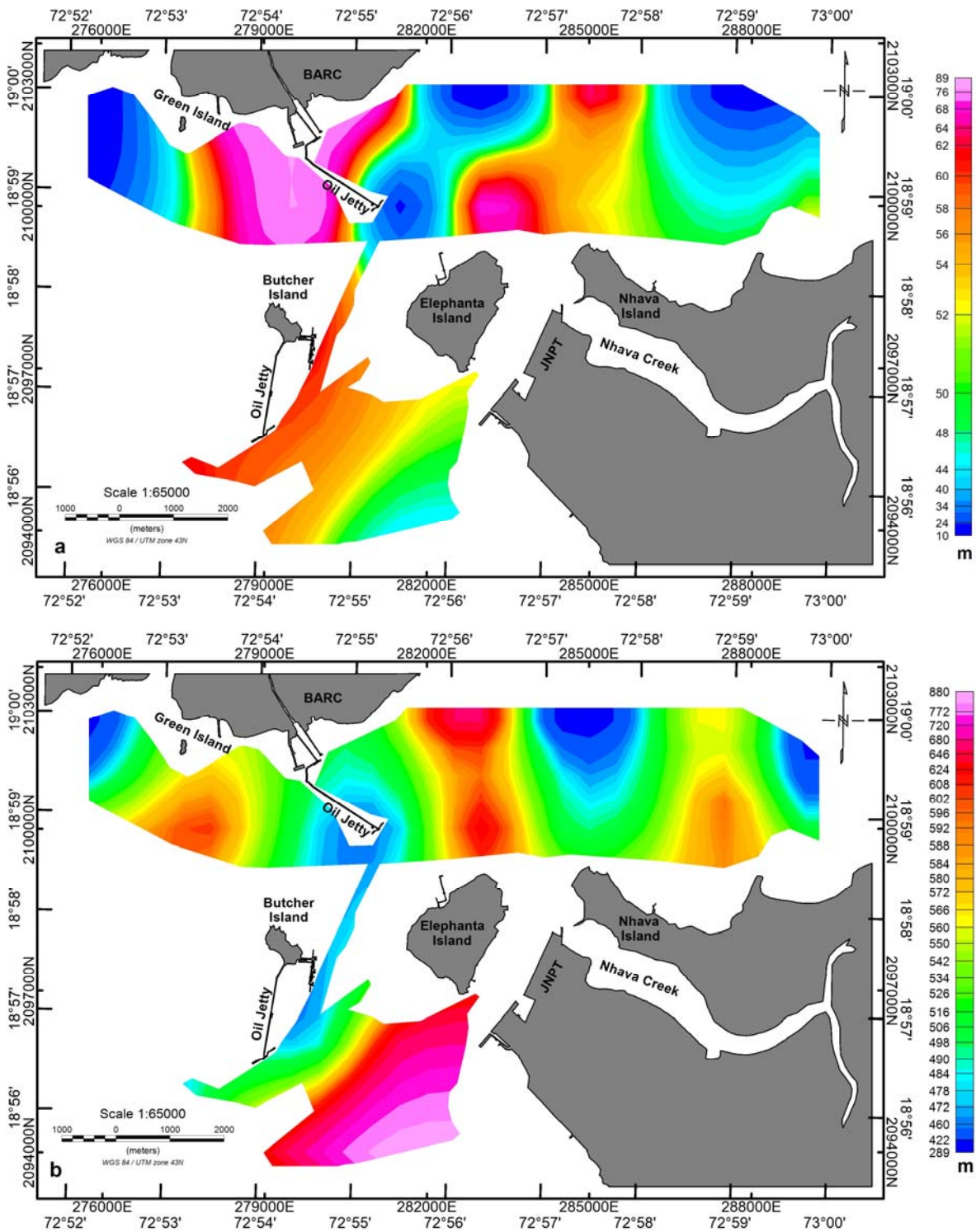


**Figure 10:** (a) Map depicting the depth to the top of the flood basalt layer, (b) depth to the base of the flood basalt layer.

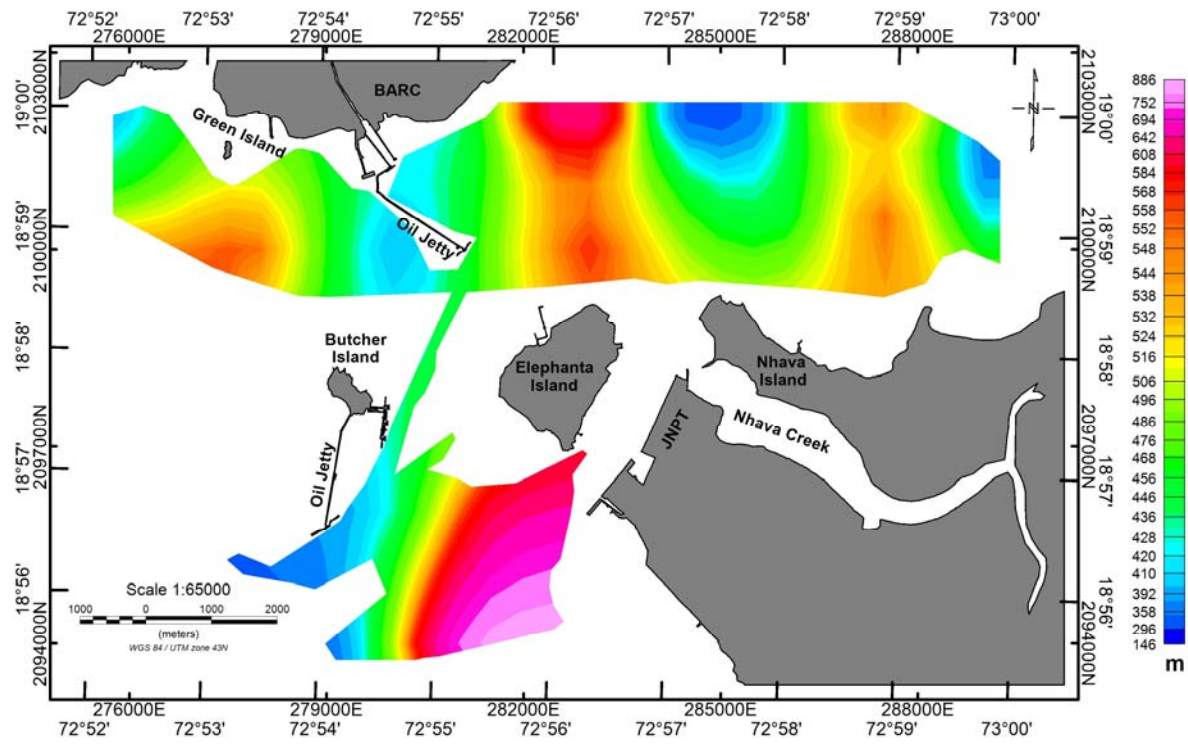


**Figure 11:** Thickness map estimated for the flow basalt in the MTC derived from the ‘depth to the top’ and ‘depth to the base’ of the flood basalt layer.

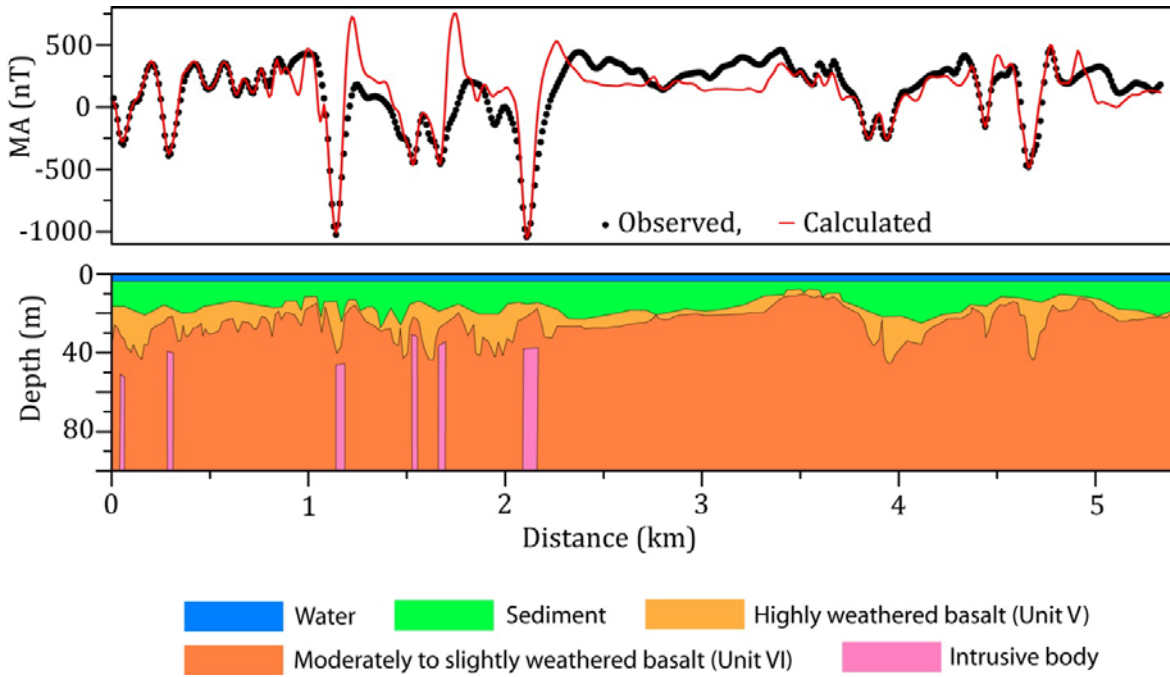


**Figure 12:** 2D forward crustal model of the MTC reaching up to 100 m depth from the mean sea level. The location of interpreted magnetic anomaly profile is shown in Figure 3b. Magnetic parameters of flood basalt and intrusive bodies for magnetic anomaly computations are taken as susceptibility 0.0017 CGS unit and remanent magnetization 0.002-0.003 emu/cm<sup>3</sup>. For normally magnetized bodies (pink color intrusive bodies), inclination is -50° and declination is -40° (Kumar et al., 2019).

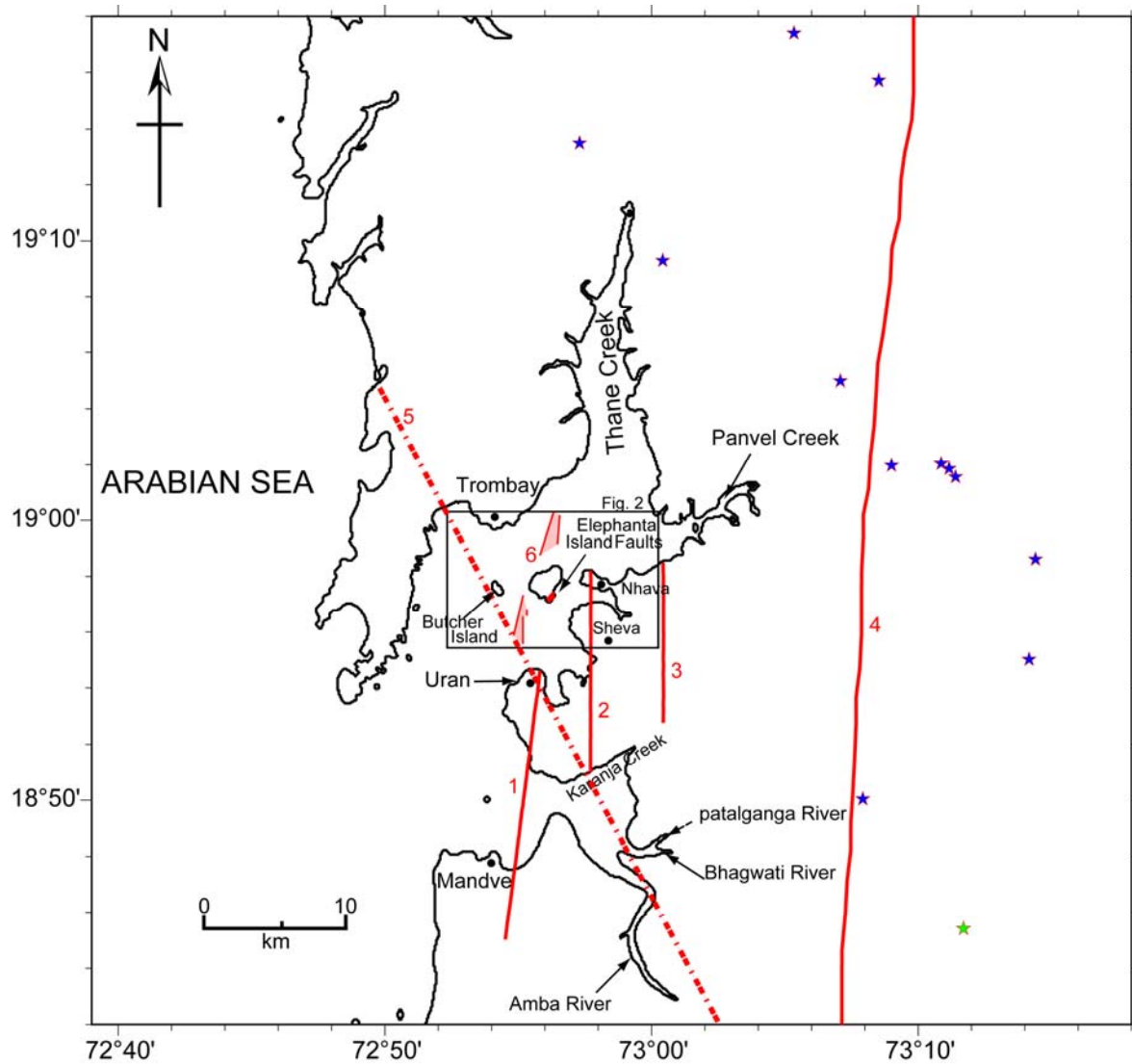


**Figure 13:** The west coast of India with the MTC represented in square box. Blue stars represent earthquake hypocenter less than 15 km and green star represents hypocenter greater than 15 km (Mohan et al., 2007). 1- Alibagh-Uran Fault, 2- Nahava-Sheva Fault, 3- Belpada Fault, 4- Panvel Flexure, 5- Uran-Dabhol Lineament (Ghodke 1978; Dessai et al., 1990; Dessai and Bertrand, 1995; Samanth et al., 2017); 6- red colure shaded region represents the marine extension of Alibagh-Uran fault zone interpreted from this study.